International Journal of Scientific Engineering and Applied Science (IJSEAS) – Volume-5, Issue-3, March 2019
ISSN: 2395-3470
www.ijseas.com

Depositional Environments, Diagenetic Processes and Hydrocarbon Potential of the Fractured Reservoir, Issaran Field, Western Shore of the Gulf of Suez, Egypt.

Ali Younis[1], Othman, A.A.[2], Mohamed Abd El-Aal[3], Emad A., Abd El Aziz*[1]

[1]Geophysical Sciences Department, National Research Centre, Cairo, Egypt.
[2]Department of Geology, Faculty of Science, Al-Azhar University, Cairo, Egypt.
[3]Department of Geology, Faculty of Education, Ain shams University, Cairo, Egypt.
* Corresponding author (e-mail: emadnrc2002@yahoo.com)

Abstract

The heavy oil in the fractured reservoir represents a large percentage of the total oil in place in the Middle East. Issaran Field, situated on the western shore of the central provinces of the Gulf of Suez, is one of the few heavy oil fractured carbonate reservoirs in the world. Three producing reservoir units: Zeit sand, upper dolomite and lower dolomite, have been produced by applying cyclic steam injection process, which considered one of the first successful cyclic steam projects in the Middle East started in 2006.

The present study is concerned with the characterizing depositional environment, studying the diagenetic processes and evaluating the hydrocarbon potentiality of the upper dolomite rock unit are the main targets of the study. The depositional environment and identification of clay minerals were estimated by using the natural gamma ray spectrometry (NGS), lithodensity log and X-Ray diffraction analysis. In addition, geologic and extensive petrographic studies were performed on some selected thin sections of rock samples representing the studied rock unit in the study area. As well as, the core, FMI image log and conventional logging should be used for fracture detection. Moreover, computer-assisted interpretation was introduced for the quantitative determination of rock constituents and evaluates the petrophysical characteristics of the studied unit.

Based on the obtained results, the upper dolomite rock unit can be discriminated into three sub-facies (A, B and C). The sub-facies "B" is the most important interval characterized by high hydrocarbon potentiality due to its

reducing environment. Diagenetic processes had a great effect on the upper dolomite reservoir quality, especially on the porosity and permeability. The sediments were deposited under shallow marine shelf conditions with an occasional more open water marine environment.

Keywords: Fractured carbonate reservoir, spectral gamma-ray, depositional environment, Western shore of Gulf of Suez, Egypt.

1. Introduction

The Gulf of Suez represents the oldest and the most economic area for the production of hydrocarbon production in Egypt, although structurally complex because of its tectogenesis. The Gulf is considered to be located between two complementary shear fractures of Suez and Aqaba that resulted from northwesterly horizontal compression. It represents a rejuvenated, slightly arcuate NW-SE trending taphrogenic depression known as the Clysmic Gulf. It is 320 km in length and is bounded by two major faults that trend NW-SE and consists of elongated troughs containing several submarine ridges (elongated structural highs). Each trough and highs have the same trend as the Gulf of Suez (NW-SE). These highs are dissected by some high-angle discordant elements that trend Aqaba trend (NE-SW) and Syrian Arc trend (ENE–WSW). These latter elements are viewed as cross faults that segment the highs (Robson, 1971, E.G.P.C., 1996 and Alsharhan, 2003).

The Gulf of Suez is a rift graben formed as a result of tectonic movements initiated in the Oligocene, which continued with intensity until Post-Miocene times. The rift is divided into three provinces characterized by different fault polarity: the northern and southern dip provinces, where normal faults dip predominantly to the northeast and the strata dips to the southwest; and the central province, where normal faults dip predominantly to the southwest and strata dips to the northeast. The dip provinces are separated from each other by rift-transverse accommodation zones (Moustafa, 1997).

The Issaran Field discovered in 1981 is located 290 km southeast of Cairo and 3 km inland from the western shore of the central province of the Gulf of Suez covering an area of 20000 acres (Fig. 1). The upper dolomite zone is a depleted fractured dolomite reservoir with 10-12 API heavy oil consists of 10% H_2S, 10% CO_2, and asphalting content around 15% with a viscosity up to 4000 cp at standard conditions. The top of reservoir depth is about 1000 ft, with an average reservoir thickness of about 400 ft and an average pressure of 250 Psi with 120 °F (Samir, 2010**)**. Due to the depletion of the reservoir by primary means, cyclic-steam stimulation was applied. Therefore, the oil recovery factor from this reservoir reached 20 % compared with about 1 % under natural depletion.

In 2003, Scimitar Production Egyptian LTD initiated a reservoir engineering study to evaluate enhanced oil recovery (EOR) in the upper dolomite unit of Issaran oil field because of its major heavy oil accumulations and low estimated primary recovery of less than 1%. In 2004, the company conducted a successful cyclic-steam stimulation pilot in well Issaran-44 (Abu El Ela, et. al., 2008). Cyclic-steam stimulation is one of the most common thermal processes in use. It involves injecting steam and then producing oil for the same well and is considered an economic oil recovery method. In 2007, production rates increased to 4000 BO/d up from 50 BO/d under primary recovery.

The Lower Miocene clastics units unconformably overly the Pre Miocene Formation in the structural lows between tilted fault blocks or over tilted surfaces of fault blocks in the Gulf of Suez and in the northern part of the red sea. High energy carbonates buildups were developed along the high edges of the uplifted fault blocks. The Middle Miocene is characterized by the development of evaporitic series, particularly in the graben areas of the Gulf. Thick anhydrites and calcareous sequences formed along the margins of the grabens giving way to thick salt basinward. The thickest salt is present near the junction of the Gulf of Suez and the Red Sea. The Middle Miocene represents a drastic change in the cycle from the heavy fluvial systems of the Lower Miocene clastics to extremely arid

conditions of the evaporite sequences (E.G.P.C., 1996). The distribution of the Miocene sediments in the Gulf of Suez is closely related to the regional tectonic setting. The Syn-rift Miocene sediments show rapid lateral variations in facies and thickness due to differential movements in the Precambrian fault blocks (Sellwood and Netherwood, 1984).

The stratigraphic succession of the Gulf of Suez has been divided into three major sequences relative to the Miocene rifting events; post-Miocene units (Post-rift); Miocene units (Syn-rift) and Pre-Miocene units (Pre-rift). These units vary in lithology, thickness, areal distribution and depositional environments. The major Pre-rift and Syn-rift source rocks have potentials to yield hydrocarbons (Alsharhan, 2003).

The aim of this study is the evaluation of the depositional environment, vertical and lateral facies variation by using spectral gamma-ray (SGR) techniques and diagenetic processes of the upper dolomite reservoir that have a great effect upon the reservoir quality hence the oil potentiality. During the last decades, the application of well logging techniques, especially SGR logs in evaluating the depositions of geological formations had been successful.

Further to the available conventional logs and seismic data, the spectral gamma-ray log and core rock samples can be used to study the lithology, evaluate porosity types and diagenetic processes in rock units. The relative contribution of the three radioactive components (U, K, Th) which differentiated with SGR logs, is particularly tool useful for the defining the lithology, depositional environment, the diagenetic history, stratigraphic surfaces and the petrophysical characteristics of the rock (Schlumberger, 1989).

2. Stratigraphy

The Miocene lithostratigraphic sequences of the Gulf of Suez province have been studied by many authors such as Said (1962); Ghorab and Marzouk (1969); Moustafa (1976); Kulke (1982); Sellwood and Netherwood (1984); Hassan and

Khalil (1985); El Zarka et al. (1989); Said (1990); Alsharhan (2003); Carr et. al. (2003); Saoudi et al. (2012); Zuhair et al. (2014) and others.

According to above-mentioned studies, Miocene evaporites are the ultimate hydrocarbon seals, whereas the dense limestones and shale of the Pre-rift and the Syn-rift stratigraphic units are the primary seals. Stratigraphic, structural and combination traps are encountered throughout the study area. The Gulf of Suez is the most prolific and prospective oil province in Egypt, and some open acreage, or relinquished area, will be of great interest in the oil industry. The Miocene lithostratigraphic sequences were previously by E.G.P.C., Stratigraphic Committee and Subcommittee, (1964 and 1974) into two main groups, the Gharandal and Ras Malaab, and six formations: Nukhul, Rudies, Kareem, Belayim, South Gharib and Zeit. Belayim Formation is dated as Middle Miocene (Langhian - Serravallian) and sub-divided into the following four formal members arranged from older to younger; Baba, Sidri, Feiran and Hamam Faroun Members. These members are deposited in a lagoonal setting, a marine inner neritic to littoral environment, a restricted marine of lagoonal setting and an open marine setting in the central parts of the basin and tidal flat to intertidal in the marginal areas, respectively (Youssef, 1986). In the study area (Issaran Field) the Miocene section includes five rock units, namely from base to top: Nukhul dolomite, Gharandal carbonates, lower dolomite, upper dolomite and Zeit sand, which similar to a marginal facies as those observed in the deep parts of the gulf. The generalized lithostratigraphic column of the Gulf of Suez basin and the detailed of the Miocene stratigraphy of the Issaran Field are shown in Fig. 2.

The upper dolomite rock unit is considered to be the main target of the present study. It is almost entirely composed of dolomite with few thin beds of shale. Nodular anhydrite is occurred dissiminated in dolomite oras interbedd lamina. Porosity is commonly oil saturated; vuggy porosity to pinpoint porosity. Sub-vertical fractures, both open and filled with anhydrite were noted in Issaran well-1 (E.G.P.C., 1996). Studied reservoir varies greatly in thickness; where the thinnest

thickness exists on the northwestern side of the studied area with 478 ft in CSS-376 well, while the greatest thickness located in the southeastern side in CSS-307 well with thickness reach to 636 ft, by average thickness around 450 ft (Fig. 3).

3. Structural setting

The study area is situated on the shore in a relatively active tectonic zone in the Gulf of Suez, and has been studied by many authors as Rebson, (1971), Moustafa, (1976), Evans, (1988), Khalil and Mesheref, (1988), Patton et al 1994, E.G.P.C., (1996), Khalil and McClay (2001), Alsharhan (2003), Haitham et al (2009), Saoudi et. al., (2012) and others. The structural evolution of the Gulf of Suez has been controlled by two main alignments:

A) Clysmic trend: parallel to the Gulf of Suez and oriented northwest-southeast trend.
B) Aqba trend: parallel to the Gulf of Aqba and oriented northeast-southwest trend.

Issaran Field was affected by the structure of the central dip province of the rift, where the characteristic feature of that province is the Pre-Miocene shallow structures underlying the Miocene sediments. The regional dip of pre-rift and syn-rift rocks is towards the northeast. The structural setting of the study area has been evaluated by using twenty 3D seismic lines passing through the study area and represented that a set of normal faults are recognized; some of them (F2, F4 and F5) dip toward SW and the others (F1, F7 and F6) toward the NE direction while the strata dip toward the NE side forming tilted fault blocks. These sections also show enclosed a small graben and step like fault forms. The vertical fault throws for the upper dolomite rock unit is ranged from 10 to 628 ft (Fig. 4).

The structural contour depth map on top of the upper dolomite unit (done using Petrel 2009 software) reveals that, the study area is a NE-tilted fault block bounded by NW-SE oriented (clysmic trend) and N-S to NNE-SSW oriented (Aqaba trend) normal faults, forming trap door structures. The faults (F1 and F3) form a graben system structure taking the direction of NW – SE. Such a high structure exists in

the middle parts along the upthrow blocks of the major fault affecting in the study area (Fig. 5).

4. Materials and methods

The study of the upper dolomite rock unit in the Issaran field is based on 15 wells, six (6) of them have SGR logs that are used to evaluate the depositional environment and hydrocarbon potentiality.

The well log data, including spectral gamma-ray (GR and SGR), caliper, porosity (sonic, neutron and density), photoelectric absorption factor (Pe) and resistivity logs (MSFL, LLS and LLD), are available in a digital format. The selected wells cover the study area with a good geographical distribution that enables good studying of the lateral variation in petrophysical, lithological and depositional changes in the studied rock unit of the western shore of the Gulf of Suez.

A comprehensive analytical formation evaluation was applied using the Interactive Petrophysics (IP) software to interpret the basic logging data for qualitative and quantitative assessments of the petrophysical properties of study reservoir. The determination of shale content is achieved through three indicators, namely, gamma-ray log, resistivity log, neutron-density logs. In order to minimize errors, the lowest value of these indicators is likely to be very close to the actual value due to the possible existence of passive shales and radioactive minerals. Generally, each of the following indicators, such as SP, GR, Resistivity and Neutron or double curve shale indicator such as Neutron and Density logs, Sonic and Density logs, Neutron and Sonic and/or (Neutron- GR), gives an estimate of the clay or shale content which is equal to or greater than the true value. Then, the minimum value within these limits is a good approximation of shale fraction (Poupon and Gaymard, 1970; Schlumberger, 1974). For shaly rocks in the studied rock unit, several models were used to calculate the water saturation and the best results were obtained using the modified Indonesian model for laminated shales (Dresser Atlas, 1982), which has the following form:

$$\frac{1}{\sqrt{R_t}} = \left(\frac{(Vsh)^{\frac{(1-Vsh)}{2}}}{\sqrt{R_{sh}}} + \sqrt{\frac{\phi^m}{aR_w}} \right) S_w^{\frac{n}{2}}$$

Where:

Rt is the true formation resistivity in ohm-m, Rw is the formation water resistivity in ohm-m, Rsh is the resistivity in front of shale in ohm-m, Vsh is the shale content infraction, Ø is the porosity infraction, Sw is the water saturation infraction, n is the saturation exponent, a is the formation factor coefficient and m is the cementation exponent.

The conventional logging data were combined with the FMI image log of some wells, applying the qualitative response of the different logging tools. The response of various types of resistivity measurements can be utilized to indicate fractures. In reservoirs with very low porosity, the dual laterolog can greatly be affected by the presence of fractures, especially those filled by conductive mud. So, vertical, subvertical and horizontal-filled fractures can be detected by the relative increase of conductivity, which they provide. Due to its short depth of investigation, shallow laterolog log (RLLs) is much affected than the deep laterolog log (RLLd) and a comparison of these resistivities in front of fractured zones will result in resistivity ratio less than one as the shallow laterolog resistivity will be less than the deep one (Abd El-Rahman and Lashin, 2004).

The petrography of the associations and their diagenetic history have been evaluated through representative thin sections impregnated with blue dyed resin to facilitate the recognition of porosity and staining with a mixed Alizarin Red-S and potassium ferricyanide solution to allow the identification of the carbonate minerals. In addition to X-ray diffraction analysis, the natural gamma rays spectrometry (NGS), and lithodnsity log are used for the identification of clay minerals.

The lithology and depositional environments were discriminated by investigation of a core rock sample of CSS-38 well and by using some cross-plots

of U, Th and K elements, which give a qualitative determination of the deposition conditions and mineralogical composition of the upper dolomite rock reservoir. The results of the analyses SGR elements are shown in Table 1.

Rock Unit	Well name	Statistical parameters	K,%	Th, ppm	U, ppm	Th/K	Th/U	U/K	Well name	Statistical parameters	K,%	Th, ppm	U, ppm	Th/K	Th/U	U/K
Upper Dolomite	CSS-68	Min.	0.01	0.02	0.02	0.07	0.01	0.06	CSS-347	Min.	0.03	0.02	0.06	0.06	0.01	0.08
		Max.	2.97	8.98	11.06	31.57	45.70	54.46		Max.	9.73	2.18	7.15	56.43	41.10	48.33
		Mean	0.69	1.84	1.40	2.69	2.94	2.07		Mean	2.23	0.69	1.59	3.52	2.95	2.73
		St. Dev.	0.45	1.51	1.33	1.9	5.3	2.3		St. Dev.	1.53	0.37	1.16	2.9	5.2	2.7
	CSS-303	Min.	0.01	0.02	0.03	0.7	0.02	0.09	CSS-307	Min.	0.05	0.02	0.04	0.05	0.02	0.05
		Max.	2.5	12.3	7.7	58.7	36	17.5		Max.	2.6	9.7	5.6	19.7	58.2	10.7
		Mean	0.6	1.9	1.6	3.3	2	2.9		Mean	0.7	2.3	1.2	3.2	4.8	1.8
		St. Dev.	0.39	1.8	1.3	3.6	3.6	2		St. Dev.	0.4	1.6	1.0	1.7	8.6	1.2
	CSS-288	Min.	0.07	0.02	0.03	0.06	0.03	0.05	ISS-100	Min.	1.1	0.56	0.05	0.3	0.4	0.04
		Max.	2.2	8.4	5.6	10.3	69	11.2		Max.	2.9	6.3	5.6	3	55.9	2.7
		Mean	0.67	2.2	1.4	3.2	3.9	2.1		Mean	1.9	2.9	0.56	1.6	15.3	0.3
		St. Dev.	0.3	1.4	1.1	1.6	8.3	1.4		St. Dev.	0.3	1.1	0.7	0.5	13.9	0.3

Table 1: Statistical parameters of the SGR analysis of the studied wells.

5. Results and discussion

5.1. Petrography

The petrographical investigation of the studied section consists mostly of light brown, creamy white and grey white, very fine to finely crystalline, equigranular, moderately developed anhedral to subhedral dolomite rhombs grading into the snow, off white, light brown blocky to sub-blocky anhydrite. Traces of framboidal pyrite and hairy-like illites locally bridging pores are observed with minor amounts of small columnar and lath-like gypsum crystals and calcite Fig. (6).

Most of the analyzed samples from CSS-38 well are of low to moderate porosity. Identified pore types include mainly intercrystalline porosity (in-between dolomite rhombs), moldic, vuggy, fracture, intracrystalline, intergranular, intragranular and shrinkage porosity (through dissolution of glaucony) types (Fig. 7). These pores are partly to completely occlude by pore filling evaporites,

dolomite and minor glaucony. Point counted porosity values range in amounts from 0.5% to 18% by volume. Average pore sizes range from 10 to 800µm, whereas pore interconnectivities vary from very poor to moderate-good (Gamil et al, 2009).

5.2. Diagenetic processes in the upper dolomite reservoir

The identified diagenetic processes have either resulted in a decrease or an increase in porosity and therefore downgraded or enhanced reservoir quality. The detailed petrographic analysis of the core samples from CSS-38 well, according to petrographic studies by Corex Services Ltd. (2009) showed that, the sedimentary succession was affected by several diagenetic processes as follows;

5.2.1. Diagenesis in evaporates:

Three types of evaporites of the upper dolomite reservoir are recorded from core samples analysis in the studied area of Issaran Oil Field, which are fine grained (Chicken-wire), radiating laths and rectangular blocky crystals (Fig. 8). On the other hand, the evaporitic fabric is nodular indicating an early diagenetic genesis in soft sediments. As a result of seawater regression in Middle Miocene and moving shoreline revealing, tidal flat lands exposed to high evaporation in arid - semiarid zones. There are two main types of evaporatic diagenesis the first is the growth of nodular evaporates in host sediments and the second is replaced by secondary evaporites (Fig. 9A). All such evaporitic processes occluded the porosity in the studied samples. The growth into evaporatic laths occasionally caused disconnected intercrystalline porosity.

5.2.2 Micritization of carbonate grains:

Initial micritization of margins of the skeletal grains is observed in some samples. Figure (9B) represents a highly sulphatized intraclasts, and bioclasts-bearing micrite to microsparite. Where a photomicrograph showing evaporite at top part replacing fine bioclasts-bearing microsparite. The fine fossil fragments are dissolved, leaving disconnected moldic porosity (Blue Dye). This alteration occurs

while the grain is on the sea floor or just below, by the activity of microbes, which cause holes and filled with fine grained sediments or cement. When this activity is intense completely micritized margins can be observed (Tucker and Wright, 1990).

5.2.3. Dolomitization:

Dolomitization is clearly detected in the studied samples either occurring as beds alternating with limestone and dolomitic limestone or associated with dense evaporitic nodules. Here it is believed that two processes possibly resulted in such two modes of occurrences.

The first mode, where dolomitic beds alternate with limestone possibly reflect laterally flowing dolomitizing fluids confined to a certain horizon as given in the models of of Land (1985) and Tucker & Wright (1990). These fluids are either saline due to sea current pumping or fresh water due to mixing from fresh water recharge along deep confined aquifer. The thin section (Fig. 10A) is composed of a mixture of very finely crystalline calcite (micrite) and a clayey material. The latter is composed of crypstocrystalline to very finely crystalline undifferentiated clay minerals. Few local patchs are partly dolomitized into dolomicrite, creating local connected intercrystalline porosity.

It is very possible that the gradual shallowing of the whole sequence caused the repetition of the same model of the lateral seepage of dolomitizing fluids in order to affect another zone underling the previously dolomitized one. On the other hand, it is very possible also that dolomitization was associated with the deposition of evaporates. As stated before, dolomitization of carbonates is commonly associated with gypsum precipitation, as a result of the increased Mg/Ca ratio, and this process releases calcium ions for further gypsum precipitation (Tucker, 2001).

The dolomitization process for the studied samples played role for both enhancing and reducing the porosity (Fig. 10). In the first-stage, as a result of the filling pore spaces due to invasion by Mg-rich solutions, the pore channel porosity has been reduced (Fig. 10A).

On this stage, the obtained intercrystalline porosity is an occluded porosity for a previous inherited porosity. At the point, when the grade of the invasion increasing, the selective dolomitization process is transferred into a further developed phase of pervasive dolomitization which caused improving the pore volume by making new pore space volume with replacement for the precursor calcite crystals (Fig. 10B). The performance of this process depends specially on the efficiency of the existing pore network. The dolomite rhombs crystal size, in addition to, the clastic content preformed a further role in inhancing the intercrystalline porosity with higher porosity values for second-stage.

On third-stage, due to the increased of invasion by a Mg-rich solution, the aggrading neomorphism of the dolomicrite rhombs into dolosparite of higher crystal sizes caused the chaotic heterogeneity of the crystal size distribution in the investigated samples of third-stage and reduced the volume and radius of the pore (Fig. 10C), therefore reducing the net permeability. The permeability of carbonate rocks is usually controlled by the pore volume and type, in addition to, the pore throat distribution, which are related to rock texture. The pore types of the studied samples are characterized by; intercrystalline, moldic, vuggy, intracrystalline, intergranular, intragranular and shrinkage pore spaces. The samples of second-stage are distinguished by diagenetic enhanced pore types, while the samples of third-stage are distinguished by diagenetic reduced pore types. The first-stage samples have a midway pore type amongst second and third stages based on the genetic pore type classification of Ahr (2005).

5.2.4. Neomorphism:

Neomorphism and/or recrystallization is very common in the studied samples as most of the carbonates that are originally deposited as mudstones or wackestones with micritic matrix are now (together with the enclosed fossils and bioclasts) showing microsparitic fabric (Fig. 9D).

Tucker and Wright (1990) best interpreted the phenomenon by stating that since many carbonate sediments originally consist of a mixture of calcite and aragonite, the recrystallization term cannot properly be used to all replacement textures. Neomorphism is used instead denoting a process of replacement and recrystallization, where there has been a change of mineralogy (e.g. change of aragonite to calcite). Neomorphic processes take place in the presence of water through dissolution and reprecipitation; which are wet processes. Calcitization is, thus, a common neomorphic process, resulting in the gradual dissolution of aragonite in shell fragments and the precipitation of calcite.

5.2.5. Dissolution:

Dissolution is clearly recorded affecting fossils and bioblasts, creating moldic porosity in some core levels. It is known that individual grains may be dissolved out, especially if they are of a metastable mineralogy like aragonite, moreover, the solubility of calcite increases with increasing Mg2+ contents (Fig. 9C).

Finally, it can be stated that, micritization and neomorphic processes decreased the porosity in sediments. Dolomitization and fracturing processes caused the increase of intercrystalline porosity. Also, dissolution caused intercrystalline, moldic and cavity porosities.

In wackestone the moldic pores may become isolated as the matrix components and cements. However, in a grain supported rock aragonite dissolution of bioclasts creates biomoldic. Evaporite minerals are also prone to dissolution (Tucker & Wright, 1990).

5.2.6. Fracturing:

Fractures associated with the faulting enhance the permeability of the reservoir andgreatly increase the productive capacity of the wells. Effect of fracture intensity on oil recovery of steam injection in continuous steam injection shows that, higher fracture density results in higher early production rate, but as the fracture's oil depleted; oil productions from matrix blocks are almost the same. Also, the

fracture systems control the production of water from the field and the oil water ratio from specific wells. The most likely fluid migration into the reservoir appears to be vertical along fracture systems that plumb into the deeper Eocene and Cretaceous section. This vertical migration improves the exploration potential for hydrocarbons in deeper zones and has widespread connotations to the fluid migration along the western flank of the Suez Basin (MacKay, 2007). Moreover, there is a direct relation between oil production and the types of fractures (open, partially open and closed fractures) as well as the proximity of the fault management. In the fractured reservoir, the permeability of cracks is much greater than that of the matrix permeability, and the greatest amount of oil produced from fractured reservoirs 98% (Khelifa et. al., 2014).

Some selected thin sections show that, the some fractures are filled due to mineralization with evaporite deposits (fibrous gypsum or anhydrite) and occasionally packed with solid hydrocarbons, e.g. CSS-120 and 303 wells (Saoudi et al., 2012). Figure (9E) shows the fracturing (stage 1) in algae grain partially filled by dolomite (stage 2). Minor fracturing (stage 2) cutting through anhydrite-filled fractures (stage 1, Fig. 9F).

The combination of microspherically focused tool (MSFL), shallow and deep

laterolog resistivities (R_{LLs} and R_{LLd}) are another effective resistivity tool for fracture identification, because the laterolog measurements will represent the fractures parallel to the shallow formation resistivity. The microspherically focused tool reads very high resistivity across low permeability matrix blocks, but gives anomalous low readings for fractures. The separation between the curves of laterolog resistivities in a fractured zone is greater due to the invasion effects. The characteristics of dual laterolog have used to estimate and detect the fractured zones by Boyeldieu and Winchester, 1982, and Sibbit and Faivre, 1985.

The resistivity-ratio crossplot figure (11), showing the effect of fractures on the laterolog measurements. Analysis of crossplot revealed that, the fractured shale,

clean, massively fractured and hydrocarbon zones, respectively. All the data points are located along the unit ratio resistivity line (R_{LLd} / R_{LLs} =1) in the area characterized by its non-fracture nature. Water-filled fracture porosity will have a ratio of R_{LLd} /R_{LLs} greater than one, with R_{LLd} reading less than that expected for an equivalent amount of intergranular porosity. For hydrocarbon-bearing fractures, the ratio also will be greater than one, but the R_{LLd} value will be higher than that seen in water-filled fracture porosity. Water-bearing fractured zones plot along line A, while points plotting to the northeast of this line represent zones of significant fracture porosity containing hydrocarbons.

Good identified fractured zones are indicated in the upper dolomite rock unit, where the majority of data points are clustered in the water bearing fracture area with the increasing order of the R_{LLd} values in ISS-100 well and above the resistivity ratio line of value 2 (R_{LLd} / R_{LLs} > 2) along a trend of increasing of resistivity from the water bearing fracture area to the massively hydrocarbon and hydrocarbon bearing fractured areas. This is supported by the good and wide resistivity separations between the shallow and deep laterologs, especially in CSS-3, 7 and 303 wells.

Photographic image of the borehole wall might seem ideal for fracture evaluation, but for the image to be useful, the fracture has to intersect the borehole. If a fracture is even a few inches away from the borehole trajectory, the borehole imaging tool will not identify the fracture. Consequently, if reservoir conditions were determined based solely on such images, reservoir evaluations would be inaccurate (Waheed et al., 2001). Therefore, in addition to microscopic analyses of thin sections, the combination between conventional logs, secondary porosity, core horizontal / vertical permeabilities ratio and FMI are used for detecting the fractured zones in the upper dolomite reservoir figure 12.

This figure shows that, the several fractured zones obtained from secondary porosity, which formed as a result of dissolution or fracturing (Soto, 2012). The

secondary porosity may be regarded to different reasons, but fracturing is one good possibility, these results are supported by this SGR result. Where, one of the important applications for the spectral gamma ray log is identified of fractures that had uranium salts precipitated in them by ground-water systems (Darling, 2005). At the point, the mobility of uranium and its presence in formation waters is considered to be the cause of high uranium radioactivity in fractures and faults (Fertl, 1979; Fertl and Rieke, 1980). The zones of high uranium radiation can be detected by the spectral gamma ray log. The increase in the potassium and thorium is indicative of non-fractured rock. Some intervals appear sharp uranium peaks are observed, others intervals are not sharp peaks, but rather the slight increase may show fracture probabilities. The presence of uranium peaks along those intervals within the studied rock unit together with constant potassium and thorium radioactivity increases the probability of the presence of fractured.

Density exhibits a significant decrease around the fracture area due to increase the fluid volume in the fractured area and it less fluid density than rock density. When the pressure of formation is less than the pressure of drilling mud, the mud may penetrate the open fractures and the formation density increases. Therefore, the density increases slightly due to the presence of high density minerals in fractures. Besides, an increase in the density of the area is expected as a result of high mud pressure and high fracture density, which provides the potential of mud deposition in the fractures.

Neutron measures the hydrogen content of a formation. In a porous formation the hydrogen is concentrated in the fluid-filled pores; energy loss can be related to the formation porosity (Laongsakul and Dürrast, 2011). Therefore, the value of neutron log increases, where the amount of formation fluid increased in the fracture zones.

Photoelectric absorption factor (Pe) shows decreases and increases observed in fracture zones in studied wells. When the fractures are open and the pressure of

formation is lower than the pressure of drilling mud, the mud invaded the fractures and (Pe) increases as a result of the penetration of mud, loaded barite into the open fracture due to the atomic number of pore water particles is less than the rock minerals (Serra and Serra, 2004). If the fractures are semi-closed or closed and drilling mud can not penetrate in the fractured area. (Pe) show a lower trend around the fracture location with the peak slightly above supporting a hydrocarbon filled fracture.

FMI image logs viewed in static and dynamic views while fitting sine waves to observed bed boundaries, fractures, and other geologic features. Static images have one contrast setting for the entire well, providing a view of relative changes in rock resistivity throughout the borehole. Dynamic images have variable contrast applied in a moving window, providing enhanced views of features including vugs, fractures, and bed boundaries. Dynamic images reflect detailed features in rocks that have very low resistivity; e.g. shales, and very high resistivity; e.g. carbonates and crystalline rocks. Fractures in the subsurface analysis were characterized as either natural or induced features. They were also classified as conductive or resistive features, representing possibly open; water-filled or closed; mineralized fractures, respectively. The azimuths and dips of interpreted geologic features are presented in a tadpole plot (Fig. 12). The vertical scale is depth and the horizontal scale is dip (0°-90°).

Saoudi et al., (2012) said that, the fractures affecting the upper dolomite reservoir have been diagnosed on image logs of 59 wells in the Issaran Field are 2546 fractures. The predominant trend of fractures affecting the studied reservoir unit is NNW-NW (N15°-45°W), which forms two sets dipping in the northeast and southwest directions at steep angles with average of 65°. Other fracture trends are N-S, NNE-SSW and WNW-ESE. The southwest dipping fracture set is more dominant than the northeast dipping set and is parallel to the main fault bounding the western side of the studied area. The orientations of the fractures dissecting the upper dolomite reservoir, which identified on image logs, have been plotted on the

rose (Fig. 13). Most of these fractures are shear fractures, included open and closed fractures in nearly equal frequencies and the same attitudes. Some of the fractures recognized as mineralized on image logs might be filled with high-resistivity and high-viscosity hydrocarbons.

The relationship between faults and fracture directions in the studied area: shows that, fracture data from upper dolomite wells had been differentiated to the three groups based on their location for existing faults. The fractures neighboring, to the main NW-SE trending fault bounding the southwestern side of the area, and the vicinity of the main NNW-SSE trending fault that bounding the western side show, very good symmetry to these faults (Fig. 5B). The fractures in the wells near the WNW-ESE trending fault that dissecting the central part of the area show, different fracture directions are oriented towards WNW, NW, N-S, NE and ENE, but most of them are parallel to this fault. These different fracture orientations have led to the improvement of a network of interconnected fractures and resulted in excellent oil production from the wells drilled near this fault.

5.3. X-Ray diffraction analysis

XRD analyses by Corex Services Ltd. (2009) indicate that, the main constituents of the samples are dolomite and anhydrite. The abundances of anhydrite and dolomite range between minor to abundant amounts. Plagioclase feldspars, quartz and pyrite are detected in very minor quantities in some samples. Smectite is the only detected clay type. The percentages of minerals identified by XRD of the upper dolomite rock unit are shown in Fig.14.

5.4. Spectral gamma-ray ‘SGR’ logs analysis

The study focuses on the variation of SGR and its components in vertical and lateral dimension in the studied rock unit and its relation to the depositional environments and sedimentary facies variation.

5.4.1. Vertical variation of SGR though the upper dolomite rock unit:

The main components of spectral gamma ray log (Th, K and U) for the studied section are plotted in a vertical manner. It shows abrupt increase of the thorium, potassium and uranium components between zones "A&B" in the studied section and a gradual decrease toward the lower parts of the studied section almost in all wells. It can be noted that, the concentration of SGR components in the studied section is almost similar in all investigated wells and the remarkably abrupt change in the SGR signature at the top of this rock unit. Presentation of the spectral gamma-ray versus depth (Figs. 15 - 16) indicates that, there are three different SGR signatures through the studied wells in the upper dolomite rock unit. These signatures can be owed to the presence of three subzones named A-C. In the zone A, the uranium content is low accompanied with relatively low potassium and thorium contents whereas the ratio Th/U is high, as well as anhydrite interbedded with gypsum and sulphatized dolomitic limestone are dominated lithologic composition. So, these SGR signatures can be due to relatively shallow lagoonal environment. In the zone (Zone B), the U, Th and K contents are usually relatively high, characterize the dolomitic wackestone and mudstone intercalated by braccia, slightly argillaceous usually reflect shallow marine environment, which may be due to the exists of aluminosilicate detritus derived mainly by reworking the subaerially exposed platform surface (Ehrenberg and Svånå, 2001). In the third zone C, the U, Th and K contents are usually with relatively moderate values, which characterize dolograinstone/dolorudstone interbedded with argillaceous anhydrite. Furthermore, the dominated dolomitic composition is an indication for the deep lagoonal environment. As a result of the change on the facieses and the increasing of the natural fracture on some area, a faster break was noticed. Also, it noticed that some wells producing water only after steam, which lead to re-evaluate the petrophysical parameters and give an indication of the presence of water zones inside the formation, although all zones have high resistivities (Samir, 2010).

5.4.2. Mineral identification by "SGR" components crossplots of upper dolomite rock unit:

Two clusters of mineral samples are indicated by plotting the Th/K ratio against photoelectric cross section (Pe) (Fig. 17), where the SGR data of CSS-68, CSS-288, CSS-307, CSS-347 and CSS-303 wells plotted on the illite, chlorite, montmorillonite and mixed-clay content zones, with some data deviated towards the mica, referring to early stage of weathering. While SGR data of ISS-100 well represent another plotted on the illite, chlorite, montmorillonite and mixed-layer clay zones, minor content of glauconite with a lot of mica content, indicating an early stage of weathering. Core samples investigation of CSS-38 well emphases minor glauconite could be observed with green to brownish green glaucony pellets have been determined in few samples and range in abundances from trace quantities to 4.5% by volume. Glaucony has been observed as rounded to oval-shaped grains that are partially to complete dissolve. Some glaucony pellets have been undergone phosphatisation processes (Gmail et al., 2009).

Furthermore, the cross plot of thorium-potassium concentration (Fig. 18) reflects that, the same results of the previous cross plot (Fig. 17), on which the data are also plotted on the illite, montmorillonite and mixed-clay zones with some data deviated towards the glauconite and mica zones.

5.4.3. Depositional environment as deduced from SGR components:

The distribution of the radioactive elements: thorium, uranium and potassium, reflects the process of sedimentation and depositional environments. According to Koszy, 1956, Adams and Weaver, 1958 and Hassan, et al., 1976, the ratio of thorium to uranium is very important in this manipulation. As the marine shale has a considerable amount of uranium and the affinity of thorium for terrestrial sediments has been reported, therefore, the ratio of Th/U can give an implication on the influence of marine affiliation on the depositional environment. Depending on such ratio (Th/U), the sedimentary facies can be classified into low (below 2,

i.e. uranium-rich; uranium fixation under probable reducing conditions), intermediate (2 - 7) and high (over 7, i.e. uranium-poor; implied uranium mobilization through weathering and or leaching, and therefore indicated an oxidizing, possibly terrestrial environment); lower values indicate marine conditions (Adams and Weaver, 1958). On the other hand, place deposits reflect high ratio, in which the uranium content is removed, leaving behind thorium in high concentrations. Shallow marine conditions represent an intermediate stage between marine and continental conditions. The data plotted on (Fig. 19) show that both, high and intermediate Th/U values are present, suggesting that the upper dolomite unit was deposited under fluvio-marine conditions.

The ratio Th/U is consistently low through the upper dolomite unit, probably because U is moderate to high content. There is a broad band of the plot points of Th /K versus Th /U that can separate by two lines separated the chart into four parts (Fig. 20). The horizontal line separates between detritus and marine sediments, and the vertical line separates between enrichment and reduced organic marine sediments.

1- First plotted point part represented by a few points and high Th/K and Th/U ratios reflecting the relative abundance of Th (despite its low to moderate absolute content, as would be expected from the little what argillaceous character.

2- The second part represented by plenty of plotted points distinguished by low Th/K and low Th/U ratios reflecting the relatively low of Th and enrichment of U this confirms a good organic matter marine carbonate depositional environment with a little detritus sediment.

3- The third part represented by numerous plotted points that reflect Low Th/K ratio and a high Th/U reflects the decreasing U content and reducing of the content this confirms marine carbonate depositional environment with a little organic matter.

4- The fourth part is represented by few points distinguished by high Th/K and low Th/U ratios reflecting the relatively high of Th and reducing in U content this refers to detritus sediments. The first and fourth region represented by a few points and sign to argillaceous and clay content of the minor thin shale streaks of the examined rock unit while the majority of the plotted points close to 2&3 parts considered a good indicator to the prevailing marine depositional environment.

Thorium concentration and thorium-uranium ratio against depth (Fig. 21), shows that, the depositional environments that predominant during deposition of the studied unit, mostly marine environmental conditions, especially in the lower part, becoming shallow and deep lagoonal in the upper part. This interpretation is confirmed by the core rock data.

5.4.4. Facies description of upper dolomite rock unit:

To differentiate between the clastics and non clastics facies, the cross plot of the apparent matrix volumetric photoelectric index (Umaa, barns/ electron) versus depth have been made for the evaluated rock unit (Fig. 22). It's reveals that, the studied facies are mostly calcareous with some streaks of argillaceous sediments. This section can be considered calcareous predominance excluding the zone B that extends laterally in all wells and the lower part of zone C are argillaceous prevalent. The prevalence of marine-shallow marine and lagoonal depositional environments during the deposition of the upper dolomite unit in the studied field, was referred to by the predominance of the illite and montmorillonite, as the main clay content, in studying wells, resulting from the prevailed diagenetic conditions and post-depositional history.

The Thorium content considered an important element to discriminate between the anhydrite facies (4.2 ≥ Th ppm) and the argillaceous carbonate facies (12 ppm ≥ Th), the uranium content is a discriminates the argillaceous dolomitic wackstone facies (11 ppm ≥ U ≥ 0.4 ppm) where it is the largest response in the studied

section and the other facies give the lowest response (5 ppm ≥ U), whereas the K content may be a diagnostic to the clastics facies (3.0 % ≥ K ≥ 0.07%).

The upper dolomite rock unit facies could be distinguished into three subfacies groups (Figs. 23 and 24) as follows:

The first group A; Represents the facies that characterized by a relatively low Th content (4.2 ppm ≥ Th ≥ 0.2 ppm), low K content (1.25 % ≥ K ≥ 0.11 %) and relatively moderate U content (5 ppm ≥ U ≥ 0.2 ppm) and mostly includes mainly anhydrite interbedded with sulphatized limestone.

The second group B; Represents the facies that have a moderate Th content (9.73 ppm ≥ Th ≥ 0.04 ppm), relatively high K content (2.97 % ≥ K ≥ 0.22 %) and relatively high U content (11 ppm ≥ U ≥ 0.43 ppm) and mostly includes argillaceous dolomitic wackestone and mudstone rocks.

The third group C; Represents the facies that have a relatively high Th content (12.3 ppm ≥ Th ≥ 0.27 ppm), relatively moderate K content (2.6 % ≥ K ≥ 0.07 %) and relatively moderate U content (5.62 ppm ≥ U ≥ 0.05 ppm) mostly includes the dolorudstone and packstone interbedded by argillaceous anhydrite. The SGR signatures are supported by the core sedimentological and petrographical studies for CSS-38 well.

5.4.5. Ramifications of Th, K and U contents:

The potassium content is considered as an indication for the presence of feldspars and clay as the case of the aluminosilicate facies, e.g. the feldspathic sandstones and argillaceous limestone. Its content in the studied upper dolomite rock unit doesn't exceed 2.97%.

Figure 25 represents a cross plot of the Th versus K contents of the studied rock unit in six wells which could be distinguished into three groups, namely: Group A; Anhydrite with dolomitic limestone, Group B; Argillaceous dolomitic wackestone, Group C; Dolorudstone and packstone interbedded by argillaceous anhydrite. This figure indicates that, there is a proportional relation between them. The potassium

content is mostly increasing with increasing thorium content for most facies, where the correlation coefficient (r) is ranging respectively from (r=0.11, r=0.53 and r=0.01) for the three groups to (r=0.71, r=0.84 and r=0.72). Correlation coefficients vary in the six wells due to change in facies from one well to another. These confirm that, the group B more argillaceous than groups A and C.

The linear correlation of Th with K is indicates a strong association between Th and aluminosilicates. Uranium-enriched argillaceous facies have generally been interpreted as reflecting slow accumulation of organic-rich marine sediments under deep water, oxygen poor conditions (Swanson, 1961; Myers and Wignall, 1987 and Saller et al., 1994).

The detrital component of the total U content of shales is equivalent to one-third of the total Th content. The fraction of the bulk U exceeding one-third of the Th content to be authigenic U, interpreted to result from synsedimentary U fixation at the sediment water interface due to sorption on organic matter under anoxic conditions (Myers and Wignall, 1987). Accumulation of shallow marine sediments that rich with organic matter is attributed to the moderately U-rich argillaceous facies (Fig. 23). The content of U in the studied wells ranged from moderate to relatively high; normally, it is up to 11 ppm (Table 1), and refers to authigenic not detritus originate.

5.5. Lateral variation of SGR though the upper dolomite rock unit

Contouring the average values of SGR components of study wells (Fig. 26) reflects the lateral variation of the depositional environment of the studied section. The thorium and potassium content is the main clay indicator. Consequently, these parameters are significant for facies mapping, which is ranged from 1.8 ppm and 0.6 % to 2.9 ppm and 1.85 % respectively, and both of them take the same direction of increasing from southeastern parts to northwestern parts. While the Uranium distribution is a good indicator for dolomite and dolomitization processes and ranged from 0.55 to 1.6 ppm, and takes the inverse increasing

direction of them in the studied rock unit insuring the marine reducing environment excited in the southeastern parts, which reasonable for the oil maturation and accumulation. This confirms that the depositional setting controlled by structural setting where the marine transgression covered the deeper parts of the southeastern parts of the study area, while the clastics facies, lagoonal and shallow marine deposits tend to be near the high structure area in the northwestern parts of the studied area. The dolomite content and dolomitization processes more effective toward the southeastern parts of the study area. Core rock samples, investigation (CSS-38 well) agree with this greatly by accurate results that ranged from deep lagoon, shallow marine and marine.

5.6. Petrophysical properties of the upper dolomite reservoir

5.6.1. Reservoir properties:

5.6.1.1. Porosity and permeability:

Permeability is one of the most important factors in reservoir production, which has a direct relation with fractures in carbonate reservoirs. The relationship between core-measured porosity and permeability analyses of the studied samples from three wells of the upper dolomite reservoir are characterized by a wide range of permeability values, where the minimum value of 0.01 md is recorded, and the maximum value is 1000 md (Fig. 27). This value indicates that, permeability influenced by micro- and macro-fractures, where the aperture of the micro-fractures is generally less than 0.1mm (Anders et al., 2014). Porosity and permeability show a good positive correlation (R=0.57, 044 and 0.40 for CSS-38, CSS-303 and CSS-68 wells, respectively).

The permeability is measured in vertical and horizontal directions to show the homogeneity of the reservoir permeability in two dimensions. The cored horizontal permeability of minimum and maximum values recorded are 0.01 and 2966.02 md in CSS-38 well, while the cored vertical permeability of minimum and maximum values recorded are 0.002 md to 738.72 md in the same well.

As shown in Fig. 28, vertical permeability of the studied samples for the upper dolomite unit in CSS- 38, CSS-68 and CSS-303 wells are less than horizontal permeability. This relation indicates that, the rocks include horizontal fractures that increase horizontal permeability, which shows that the rocks in this unit are extensively fractured in a horizontal direction. Vertical fractures may not exist in these samples. The relation between the core horizontal and vertical permeabilities represent that, the relation coefficient has ranged from 0.54 in CSS-38 well to 0.93 in CSS-68 well. This relation coefficient indicates that, the permeability of the upper dolomite reservoir in CSS-68 tend to be homogenous and that of the upper dolomite reservoir of CSS-38 tends to be heterogenous, while that of CSS-303 well tends to be a mixture of both.

5.6.2. Vertical distribution of the petrophysical parameter:

A number of litho-saturation crossplots have been constructed to illustrate the vertical distribution of hydrocarbon saturation with depth. For example, figure 29 exhibits the petrophysical log data of two selected wells in Issaran Field (CSS-68 and CSS-38). These wells are selected to demonstrate the characteristics of the upper dolomite reservoir rocks, as obtained from the normal logging analysis. The petrophysical analog of CSS-68 and CSS-38 wells indicates that, the lithology of the upper dolomite reservoir is uniform and mainly dolomitic in composition with the minor anhydrite and shale content. The shale content is represented by low values, ranging from zero (clean) in all wells to 62% in CSS-68 well. The pore spaces are uniform all over the whole section, except in the upper part of the interval. They range from zero % in most well to 45% in CSS-38 well. On the other hand, high anhydrite content associated with low reduced porosity is detected in the lower part of the upper dolomite rocks in CSS-38 well. The residual hydrocarbon is shown by considerable amounts along most of the section, while the movable hydrocarbon is completely disappeared. The water is represented by minor occurrences in CSS-38 well. Based on the lithological, petrophysical and

fluid analyses, the studied interval has been differentiated into the reservoir and pay flags.

Generally, the thickness varies from 327 ft in both of CSS-10 and ISS-100 wells up to 636 ft in CSS-307 well, and it has a fair to very good reservoir potential in most study wells, where the effective porosity values vary between 10% in ISS-11 well and 30% in CSS-3 well with increasing gross thickness toward the southeastern part of the study area.

5.6.3. Horizontal distribution of the petrophysical parameter:

In order to display the lateral variation of petrophysical characteristics, a group of iso- parametric maps have been constructed for the upper dolomite rock

unit (Fig. 30):

5.6.3.1. Net pay thickness distribution map:

This map (Fig. 30A) shows the net pay thickness of oil within the upper dolomite rock unit ranges from 80 ft (ISS-11 well) to 512 ft (CSS-307 well). The net-pay of the oil is concentrated in the southeastern part and generally increases from the middle to eastern parts of the study area.

5.6.3.2. Shale content distribution map:

The shale content distribution of the upper dolomite rock unit is indicated in Fig. (30B). This map shows that, the maximum recorded shale content value is 11 % at CSS-38 well in the southwestern part, and the minimum recorded value is 2 % at ISS-100, CSS-3 and CSS-7 wells. It can be noticed that, the shale content increases toward the center of the southern part of the study area. This is the same trend of porosity decreasing, which confirms the reversible relationship between the porosity and shale content.

5.6.3.3. Effective porosity distribution map:

The map (Fig. 30C) shows a general increase of the effective porosity towards the northeastern part of the study area. The porosity values range from 10 % in ISS-11 well to 30 % in CSS-3 well. The structural elements may affect the porosity

development, but not as much as the facies of deposition, which has a great influence on the porosity. This deduction is manifested by the absence of any porosity anomalies in the porosity contour lines at or near the fault sites on the map, which implies that the effect of these faults on the porosity is minor and that, the porosity differences are fabric dependent more than structure.

5.6.3.4. Water saturation distribution map:

The water saturation distribution map (Fig. 30D) of the studied unit is affected by a Cyclic Steam Stimulation (CSS) process. As a result of the high fracture intensity, the water is rapidly channeled through the fractures. The highest water saturation value 34 % is recorded in CSS-68 well, whereas the lowest value 11 % is recorded in CSS-3 well. The general trend of water saturation increases toward the southeastern and northwestern parts of the study area (outward directions).

5.6.3.5. Hydrocarbon saturation distribution map:

The hydrocarbon saturation (Fig. 30E) decreases toward the southeastern and northwestern parts of the study area (outward directions) and increases toward the middle part along the up thrown side of the huge faults forming horst, where a lot of hydrocarbon migrations are toward the up thrown side. Oil saturations have ranged from 66 % in CSS-68 well to 89 % in CSS-3 well in the study area.

6. Conclusions

Upper dolomite reservoir due to its shallow depth, API heavy oil with a viscosity up to 4000 cp at standard conditions, the low pressure (250 psi) and low reservoir temperature 120 °F the oil is not produced as cold production. So, thermal oil recovery method is used with the intention of reducing oil viscosity in the reservoir, increasing its mobility and allowing better displacement to the producing well. The geological setting and petrophysical properties of the upper dolomite rock unit in the Iassarn Field indicate a great variation in thickness ranging from 327 ft at the northwestern part to 636 ft at southeastern parts. Thickness of the upper dolomite unit increases towards the southeastern part of the

study area, while the thinning parts occupy the northwestern parts. The highest structure exists in the middle parts along the upthrow blocks of the major fault affecting in the study area.

The facies variation of the studied rock unit has been discriminated into three subfacies according to its content of SGR components U, K, and TH and the ratio Th/U. The shale of the studied rock unit is composed of illlite, chlorite, montmorillonite and mixed-clay minerals, minor content of glauconite with a lot of mica content. The depositional environment has been evaluated as lagoonal to shallow marine and marine environments with reducing condition, especially in the subfacies 'B' that contains a large U content which is consequently, favorable for the hydrocarbon potentiality. Different diagenetic features have been evaluated in the investigated reservoir rock, which has a great effect on the reservoir quality, especially on the porosity and permeability. Most of the effective porosity of the studied rock unit is mostly of secondary origin due to diagenetic effects that reflected from the petrographic study.

The well-log analysis revealed a great heterogeneity in the petrophysical properties of the reservoir rock. The study showed that conventional logging has a good possibility to be used in fracture reservoir characterization correlated with fracture data from the FMI image log. Petrophysical characters indicate a good reservoir rock (10 % ≤ Ø ≤ 30 %) with the shale volume ranging from 2 % to 11 %; the water saturation < 34 %, whereas the net-pay thickness ranges from 80 in ISS-11 well to 512 ft. in CSS-307 well. Both the shale content and the water saturation of the upper dolomite rock unit decrease towards the central (high horst block) and the north eastern (high step block) parts of the study area. This indicates that the reservoir characteristics of the studied rock unit have been affected by both the structural and sedimentlogical processes.

International Journal of Scientific Engineering and Applied Science (IJSEAS) – Volume-5, Issue-3, March 2019
ISSN: 2395-3470
www.ijseas.com

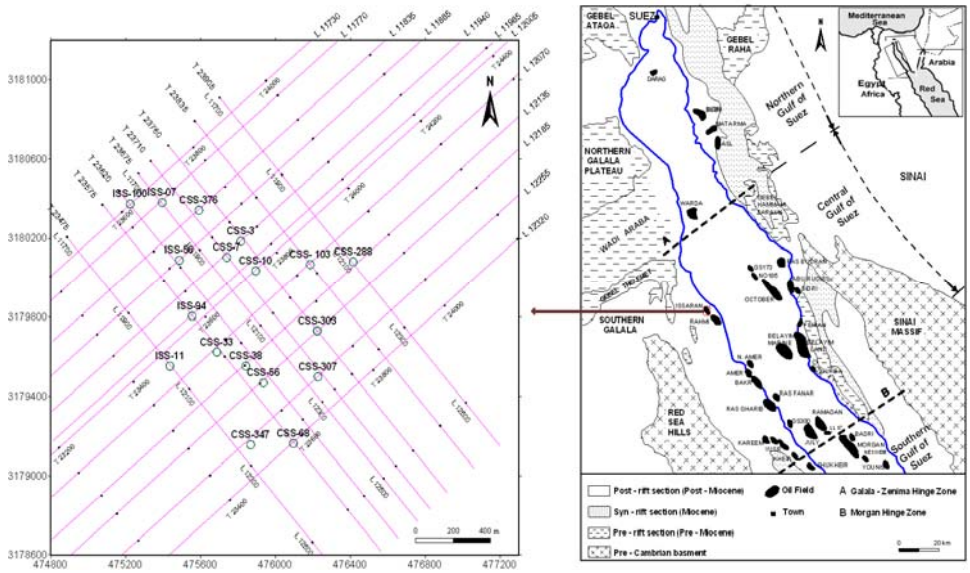

Fig. 1: Location map showing the selected wells and seismic lines of the Issaran Field, Western shore of the Gulf of Suez, Egypt.

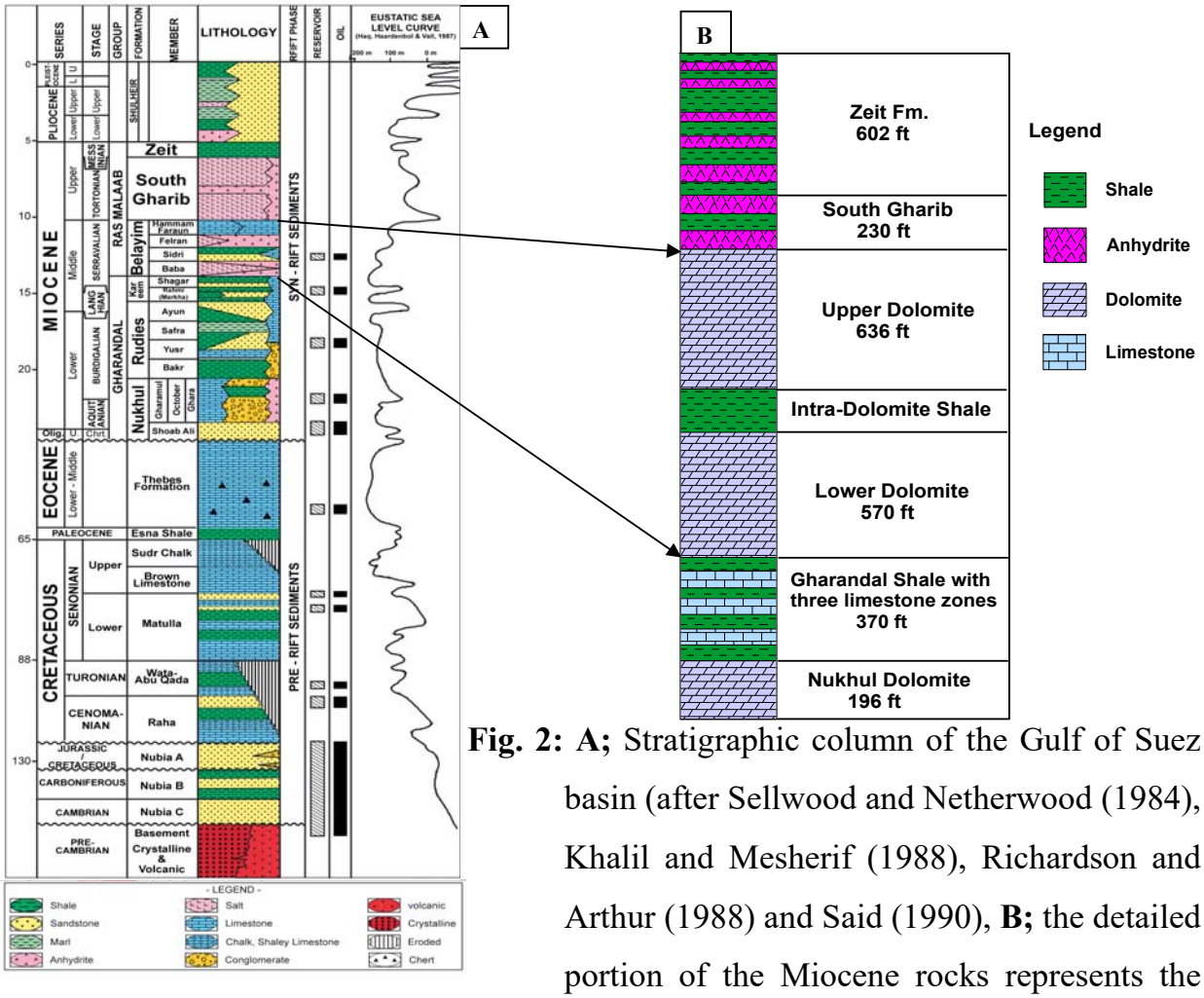

Fig. 2: A; Stratigraphic column of the Gulf of Suez basin (after Sellwood and Netherwood (1984), Khalil and Mesherif (1988), Richardson and Arthur (1988) and Said (1990), **B;** the detailed portion of the Miocene rocks represents the Miocene stratigraphy of the Issaran Field.

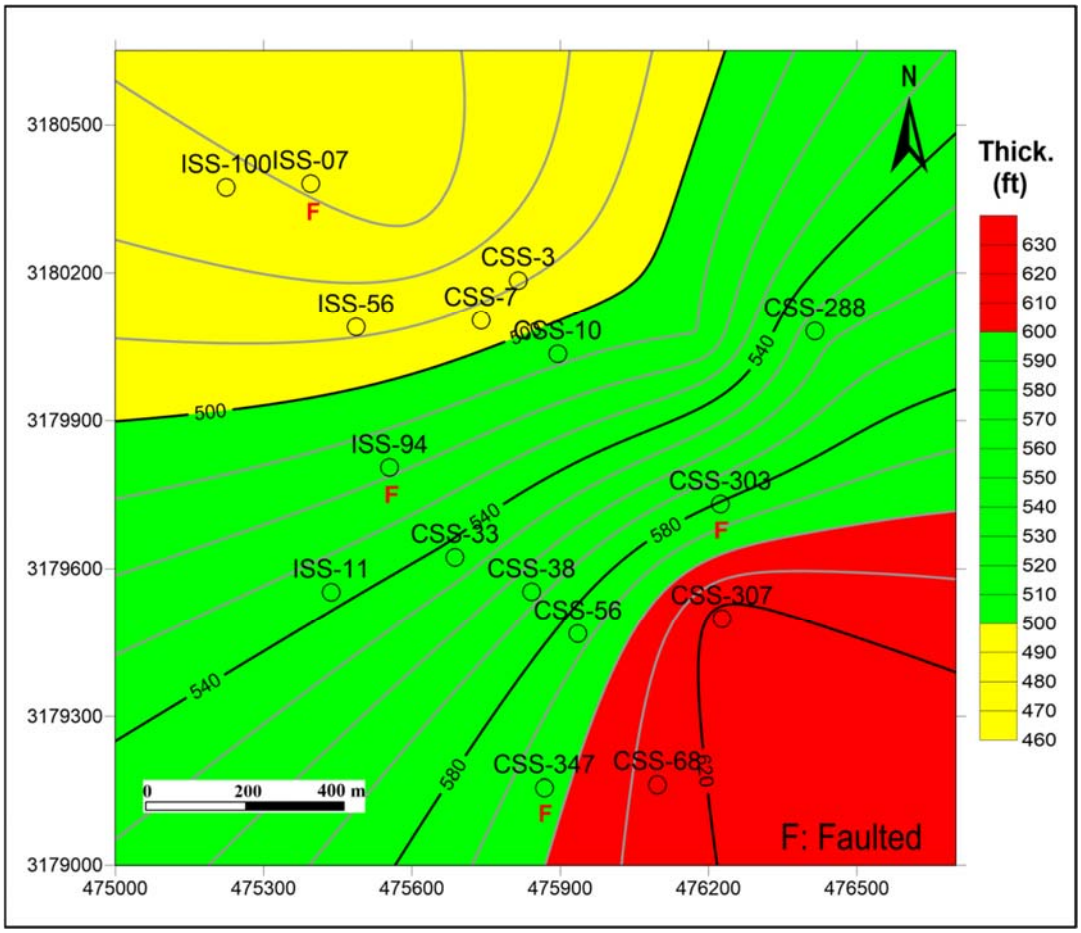

Fig. 3: Isopach map of the upper dolomite rock unit, (C.I = 20 ft.).

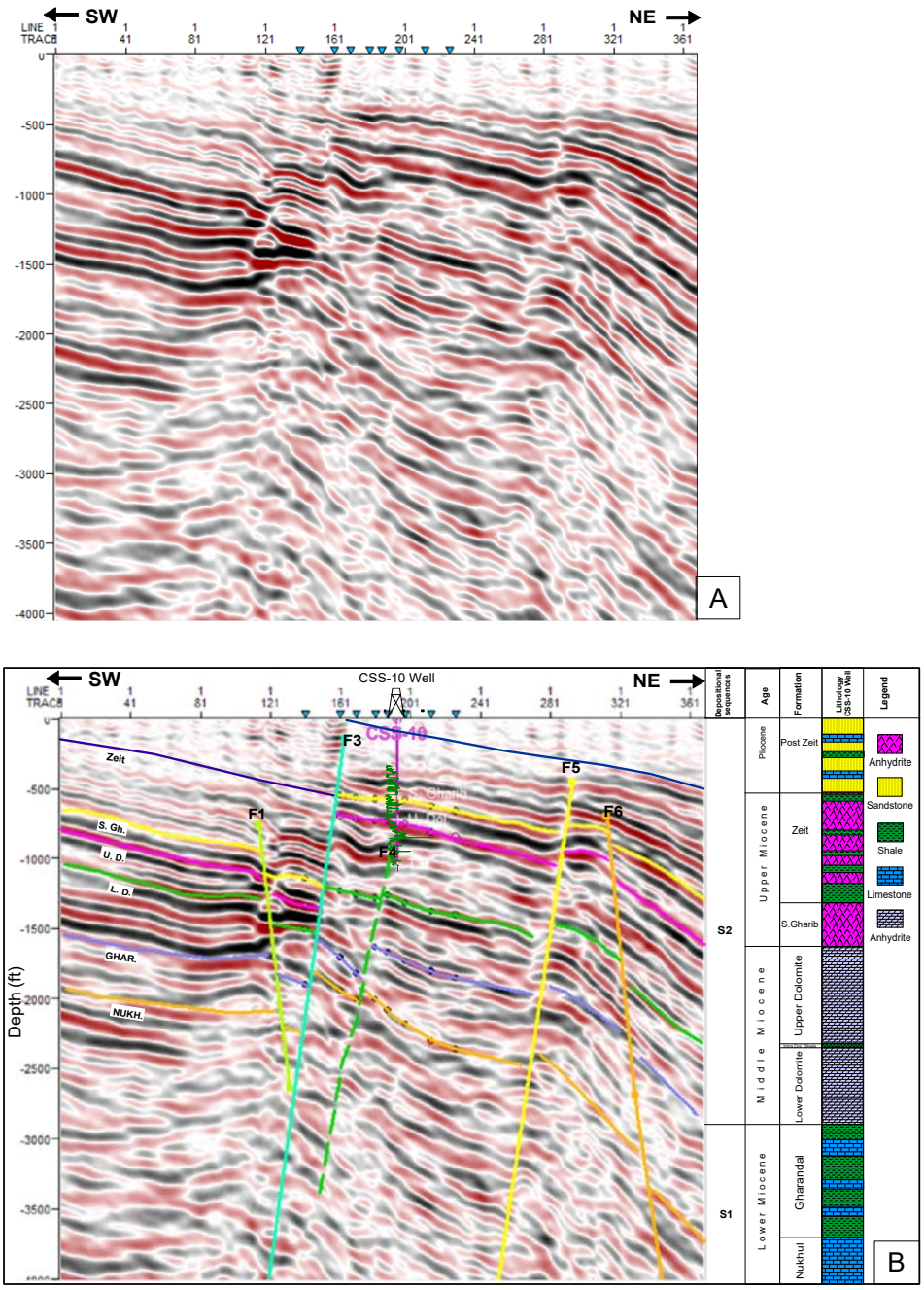

Fig. 4: A; Un interpreted seismic reflection profile (L12005) **B;** The interpreted seismic reflection profile (L12005) showing the identified structural elements.

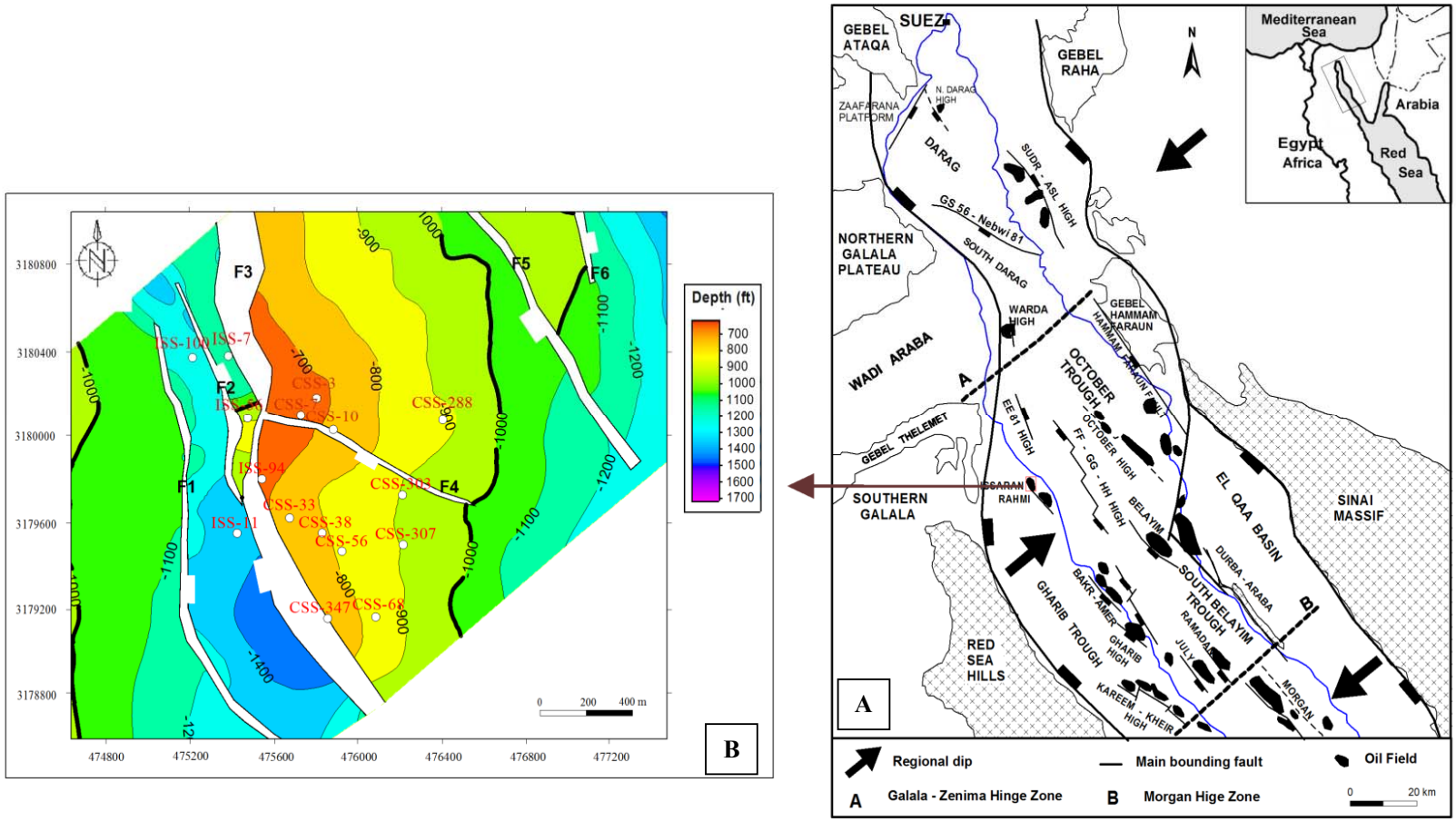

Fig. 5: A; Major tectonic elements in the northern and central Gulf of Suez (based on information from Tewfik, 1988, Alsharhan, 2003) and **B;** Structure contour depth map on top upper dolomite rock unit, (C.I. = 100 ft.).

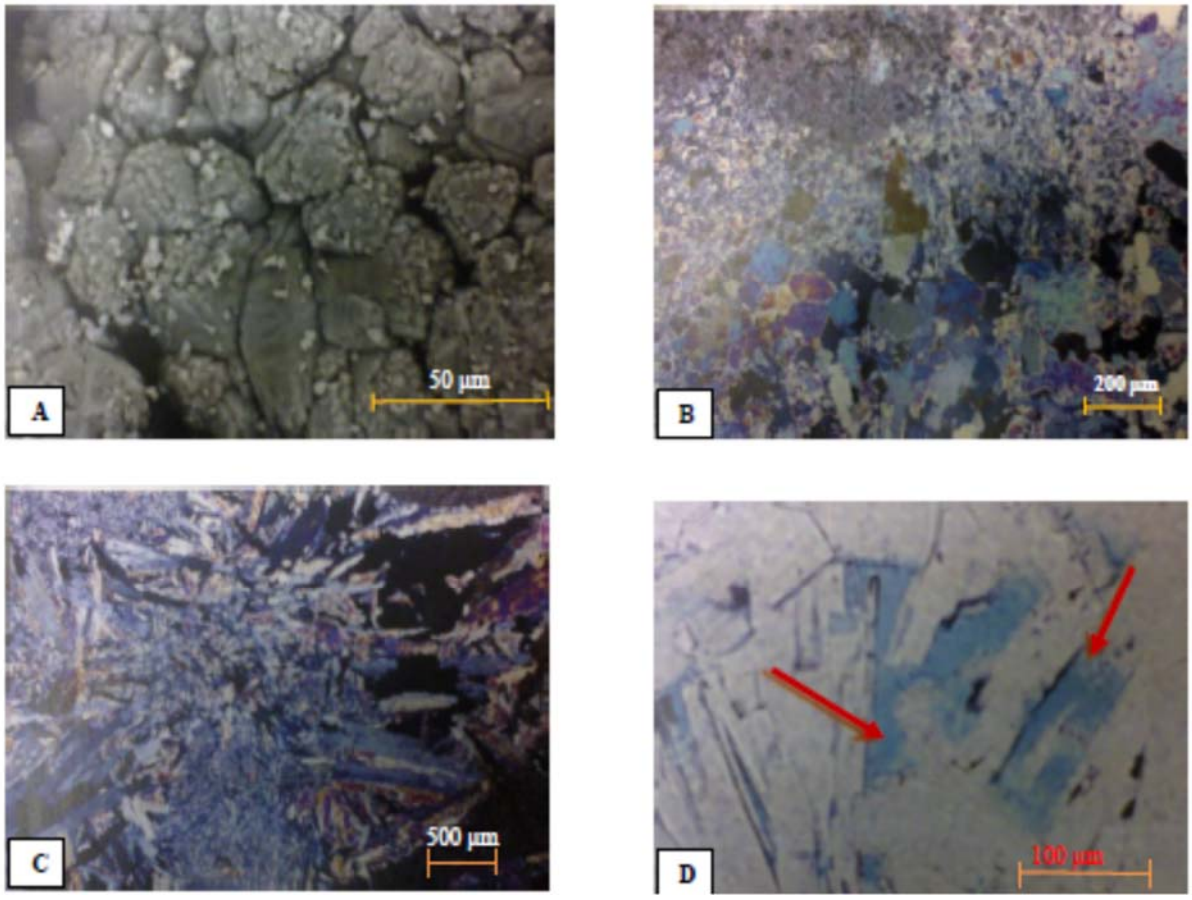

Fig. 6: Lithology of upper dolomite rock unit: **A;** Crystalline dolomite, **Depth:** 1260.06 ft. **B;** Crystalline dolomite and anhydrite, **Depth:** 1382 ft. **C;** Anhydritic crystalline dolomite, **Depth:** 1455.02 ft. **D;** Anhydrite nodules, replaced partly by gypsum, **Depth:** 1489.1 ft.

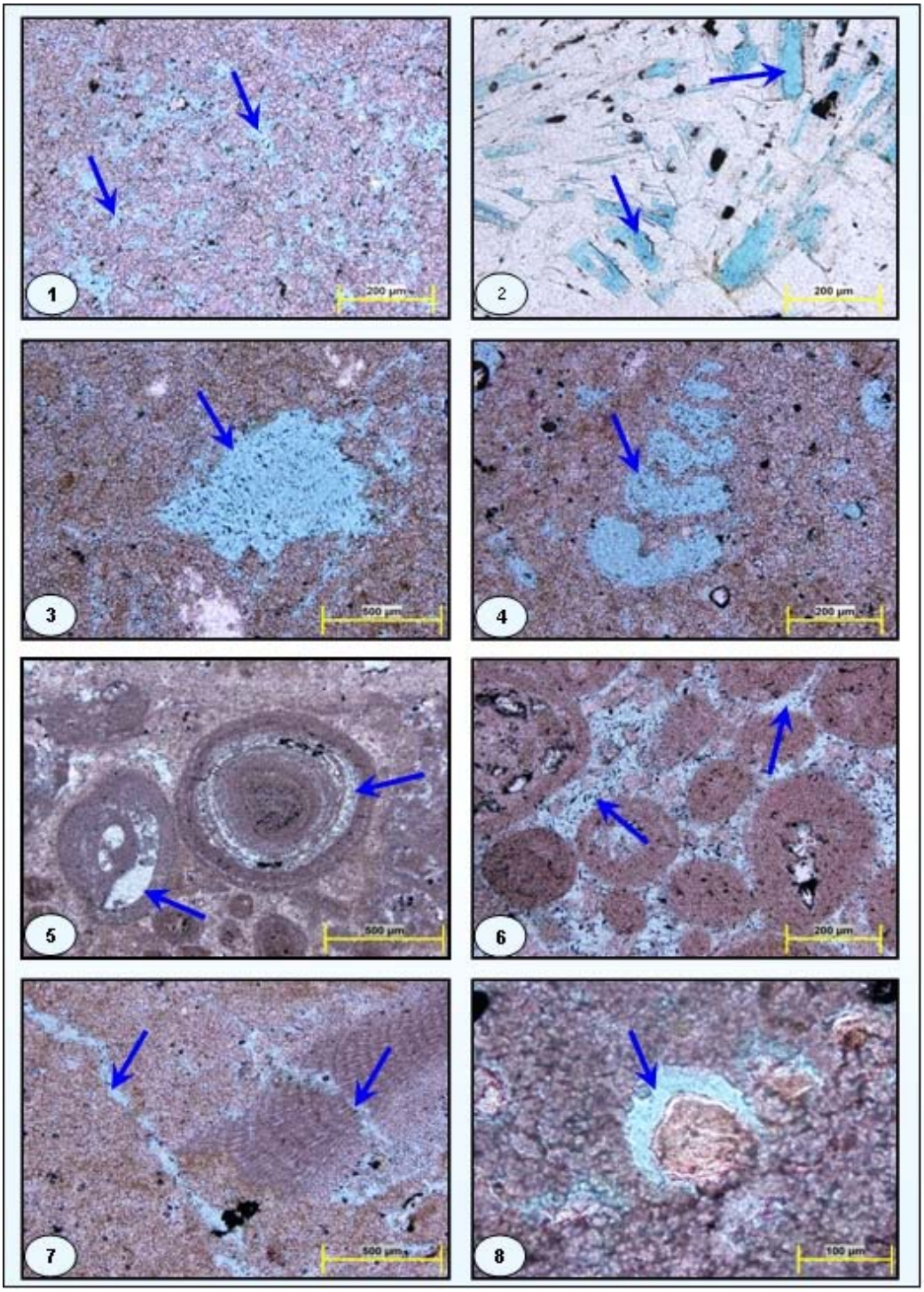

Fig. 7: Porosity types of the upper dolomite reservoir (1) Intercrystalline, **Depth:** 1324 ft. (2) Intracrystalline, **Depth:** 1489 ft. (3) Vuggy, **Depth:** 1460.02 ft. (4) Moldic, **Depth:** 1251.10 ft. (5) Intragranular, **Depth:** 1254.08 ft. (6) Intergranular, **Depth:** 1260.06 ft. (7) Fracture, **Depth:** 1342.08 ft. and (8) Shrankage, **Depth:** 1196.02 ft.

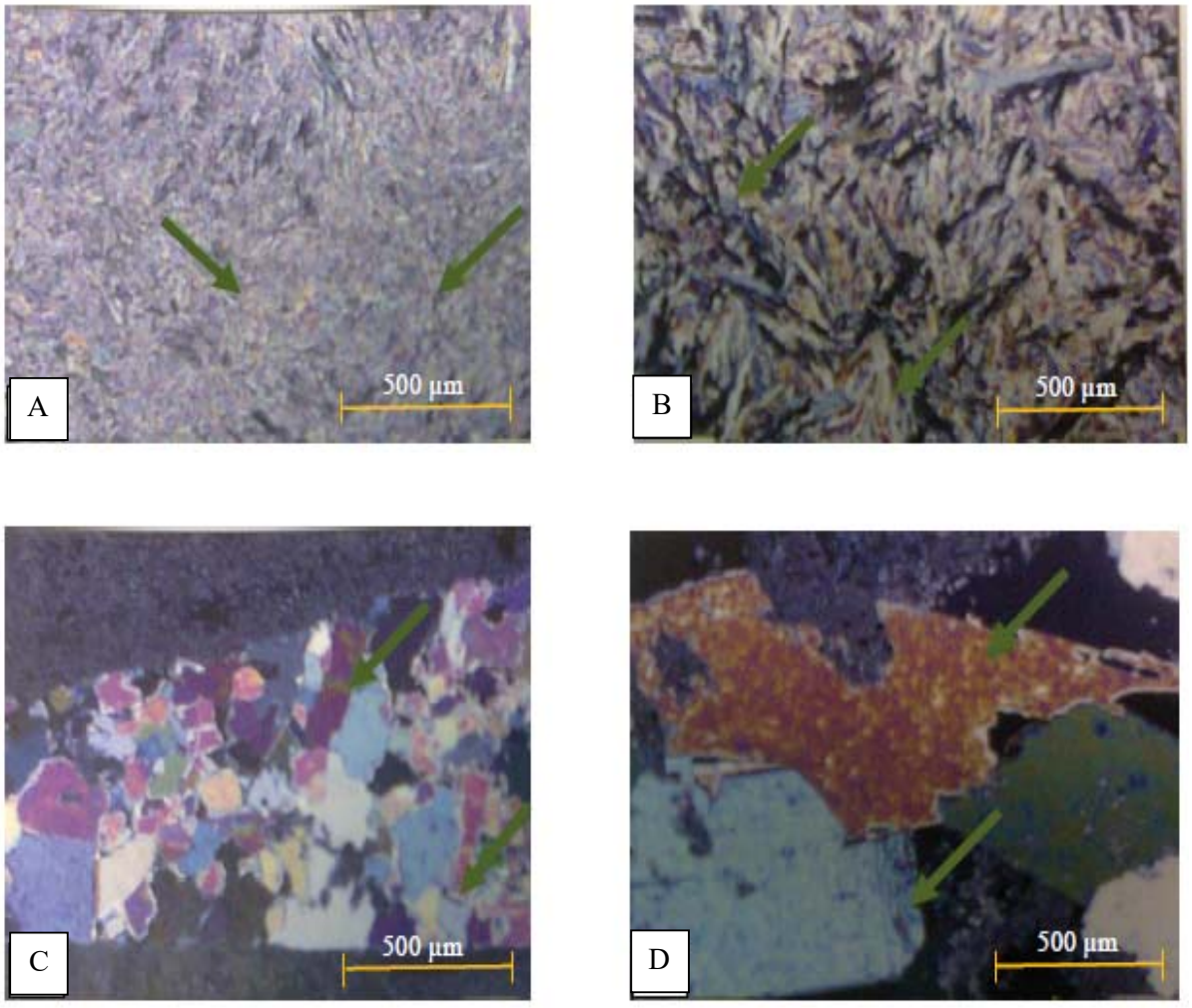

Fig. 8: Forms of Anhydrite: **A;** Fine grained (Chicken-wire), **Depth:** 1449.10 ft. **B;** Radiating laths, **Depth:** 1346.04 ft. **C** and **D;** Rectangular blocky crystals respectively, **Depths:** 1254.10 and 1361.06 ft.

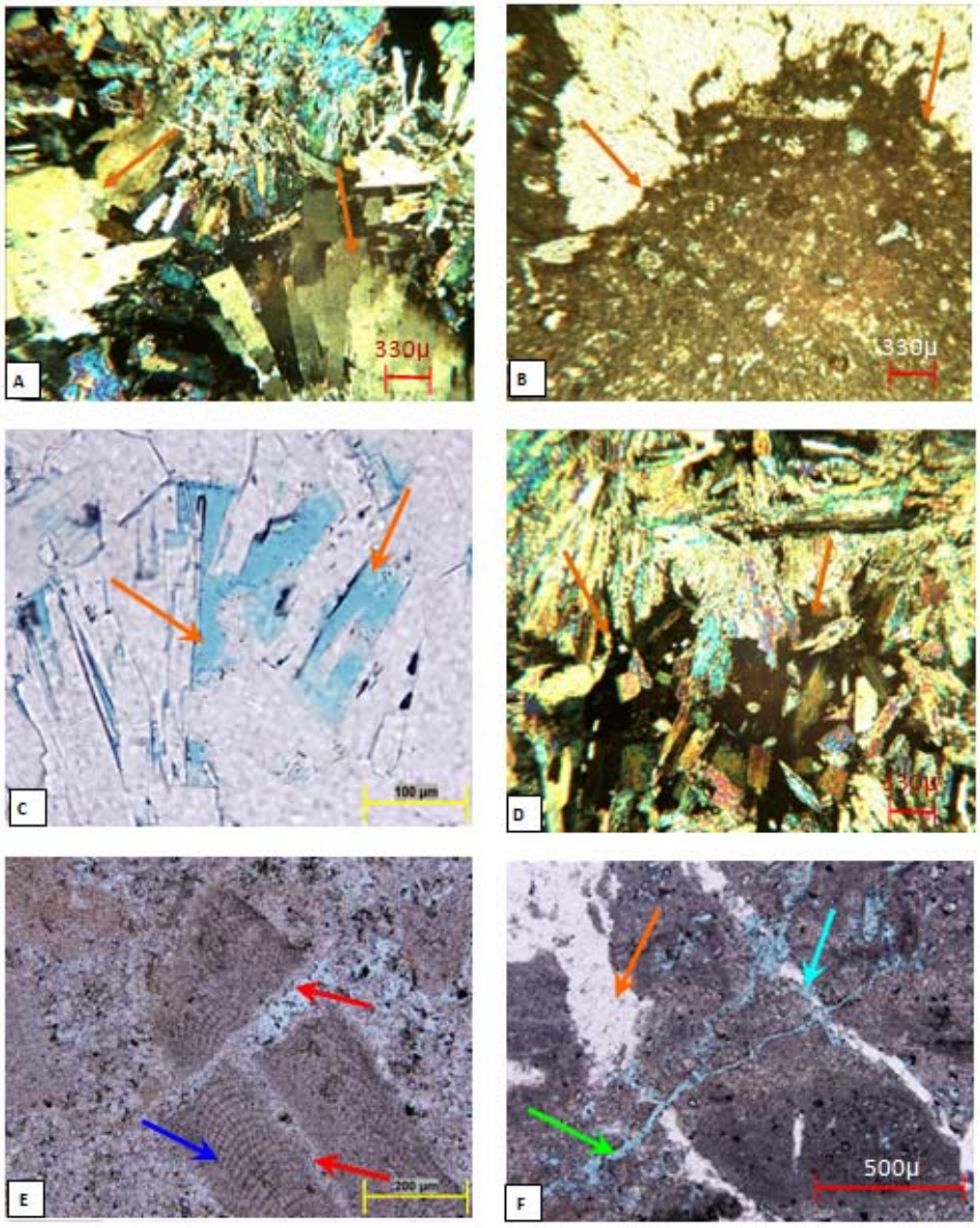

Fig. 9: Diagenetic processes in upper dolomite rock unit: **A;** Coalescing anhydrite nodules, replaced partly by gypsum with scattered dolomite crystals, **Depth:** 1053.02 ft. **B;** Highly sulphatized intraclasts-, and bioclasts-bearing micrite to microsparite, **Depth:** 1044.02 ft. **C;** Partial dissolution of evaporate, **Depth:** 1489.1 ft. **D;** Coalescing anhydrite nodules, replaced partly by gypsum with scattered remnants of "microsparitic crystals", **Depth:** 1046.03 ft. **E;** Fracturing (stage 1) in algae grain partially filled by dolomite (stage 2), **Depth**: 1342.08 ft. **F;** Minor fracturing (stage 2) cutting through anhydrite-filled fractures (stage 1), **Depth:** 1430.04 ft.

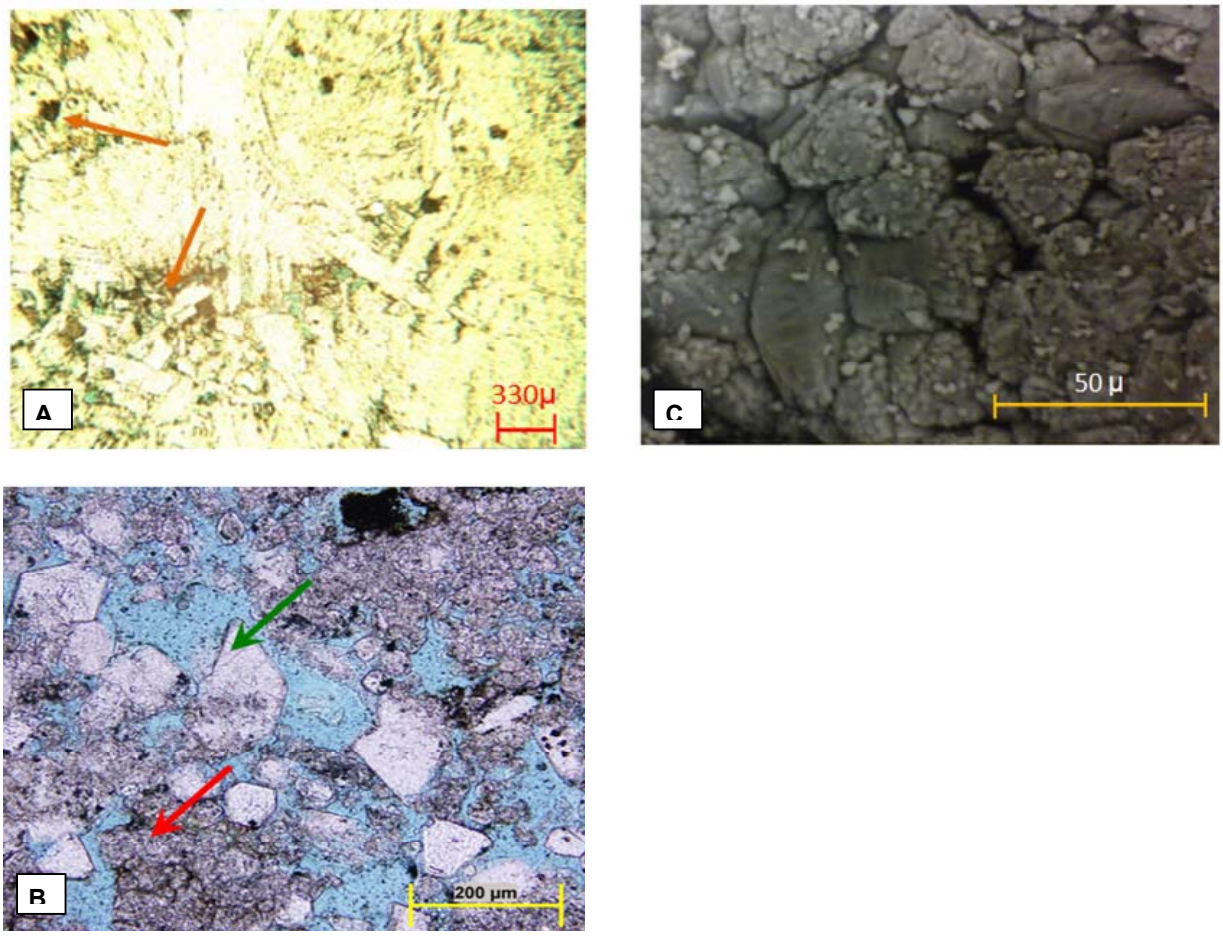

Fig. 10: Phases of dolomitization processes in upper dolomite rock unit: **A;** Coalescing anhydrite nodules, replaced partly by gypsum with scattered dolomite crystals, **Depth:** 1055.04 ft. **B;** Crystalline dolomite, fine to medium crystalline dolomite (stage 2) is followed by coarser dolomite (stage 3), **Depth:** 1324.00 ft. **C;** Crystalline dolomite, **Depth:** 1260.06 ft.

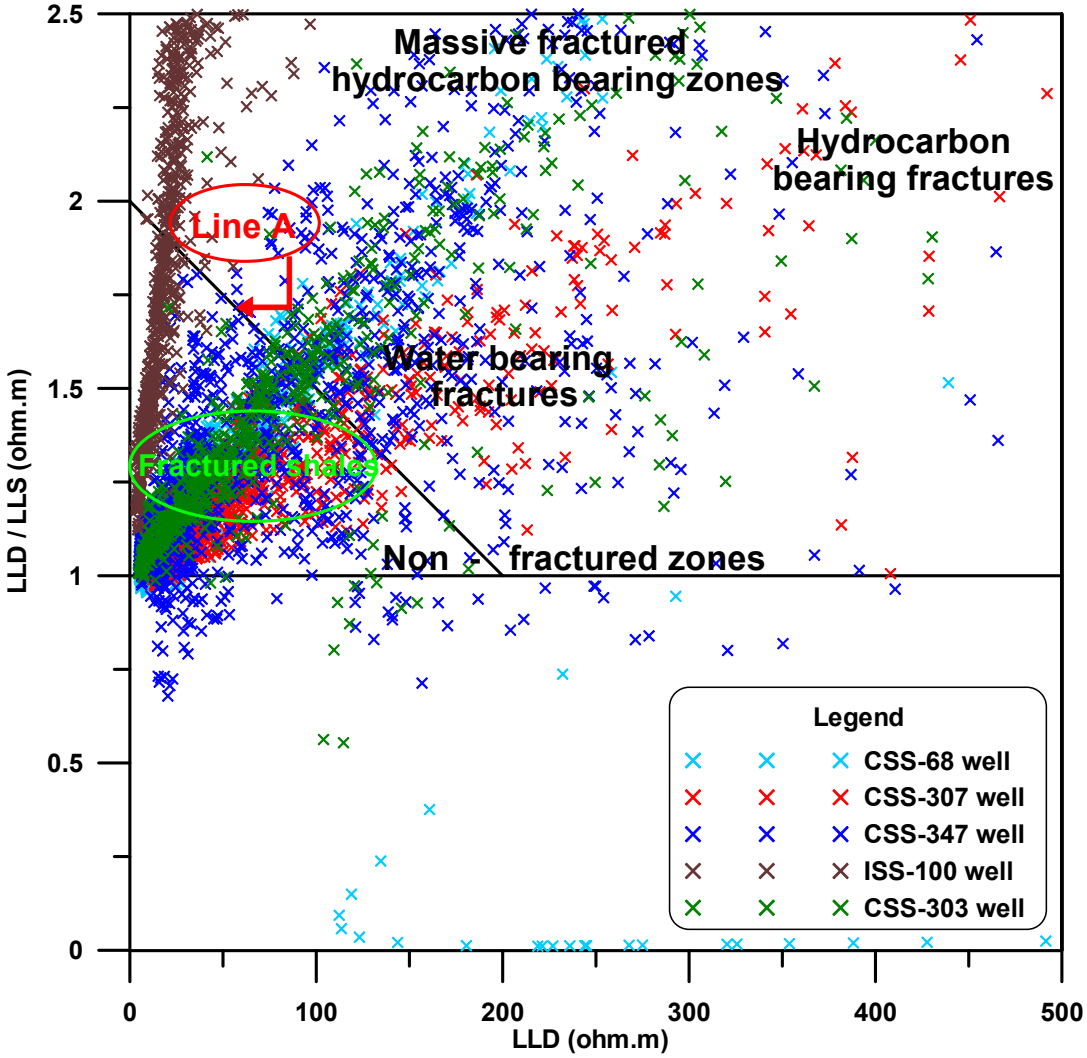

Fig. 11: Crossplot of LLD/LLS versus LLD differentiated between fractured and unfractured zones in the upper dolomite rock unit.

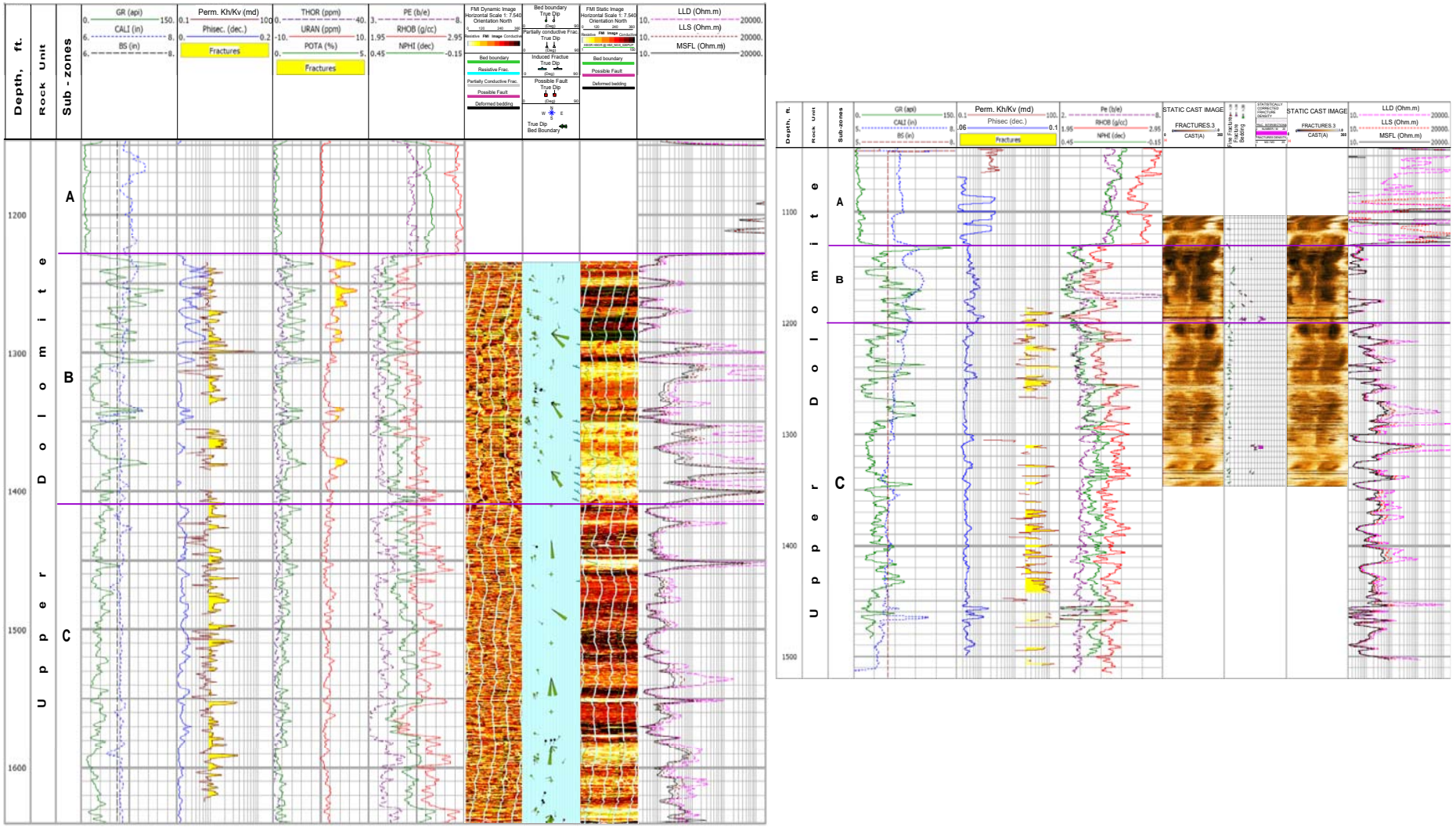

Fig. 12: The combination between conventional logs, secondary porosity, core horizontal / vertical permeabilities ratio and FMI for detecting the fractured zones in the upper dolomite reservoir, CSS-38 and CSS-68 wells.

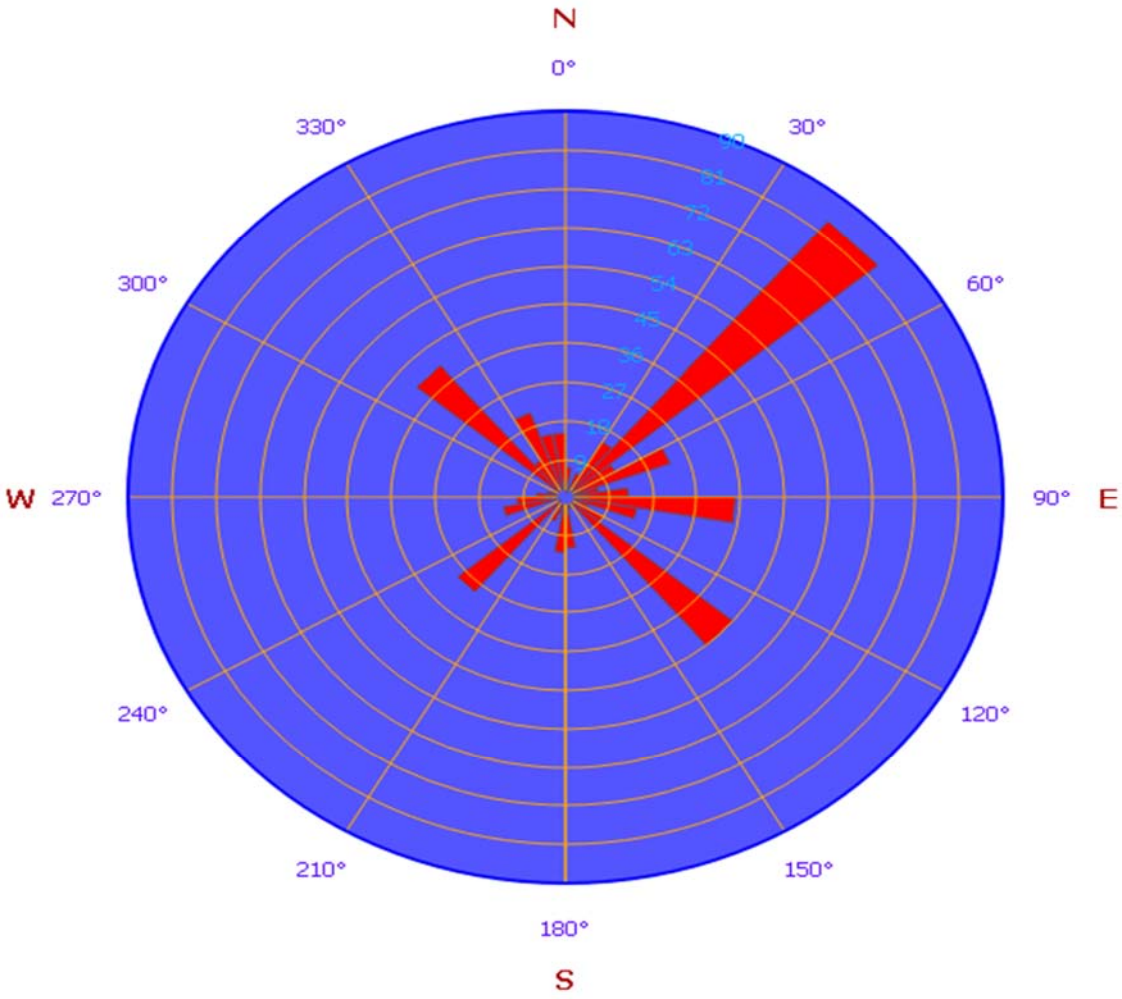

Fig. 13: The orientations of the fractures dissecting the upper dolomite reservoir, which identified on image logs based on data of CSS-38, CSS-68 and CSS-303 wells.

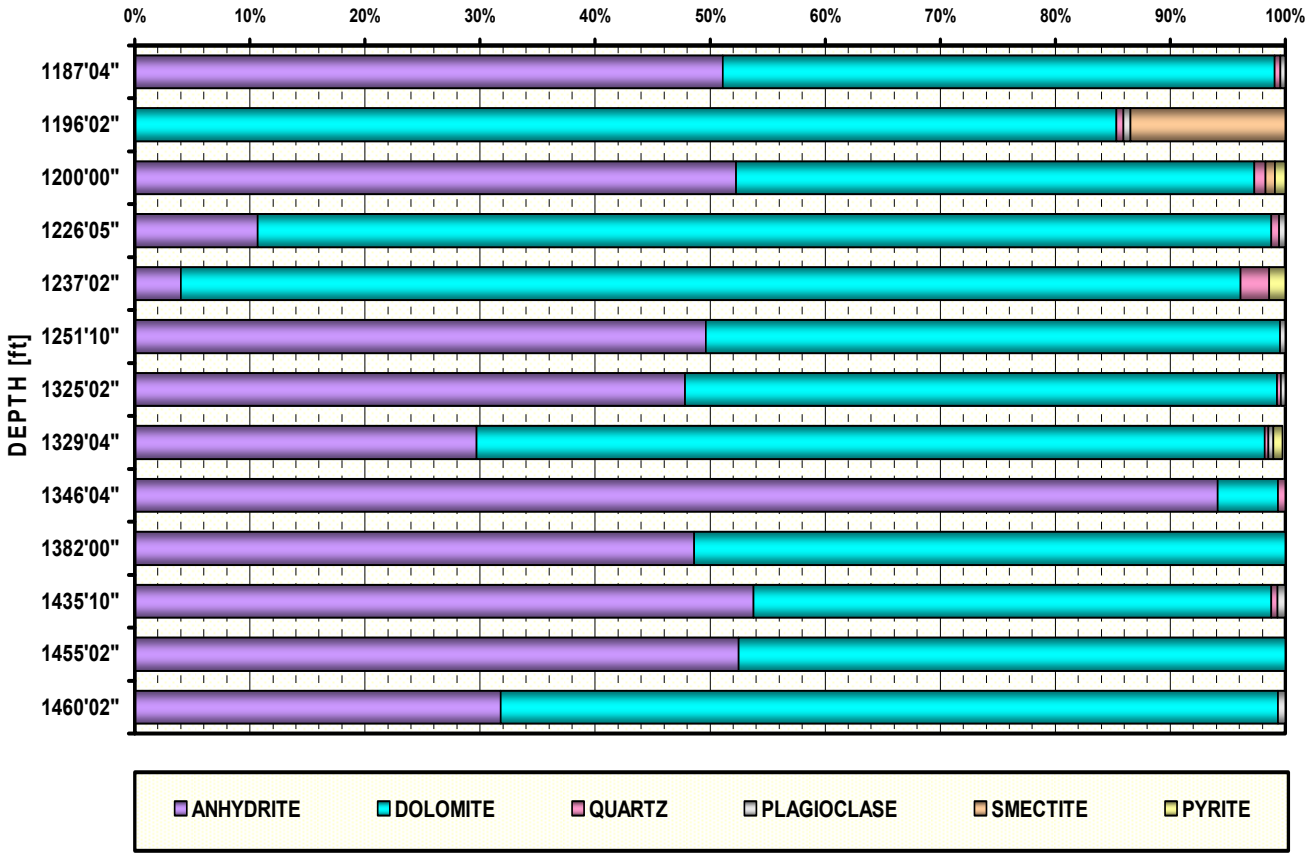

Fig. 14: X-Ray Diffraction (XRD) results sketch for core rock samples analysis in weight percent of the studied upper dolomite reservoir, CSS-38 well.

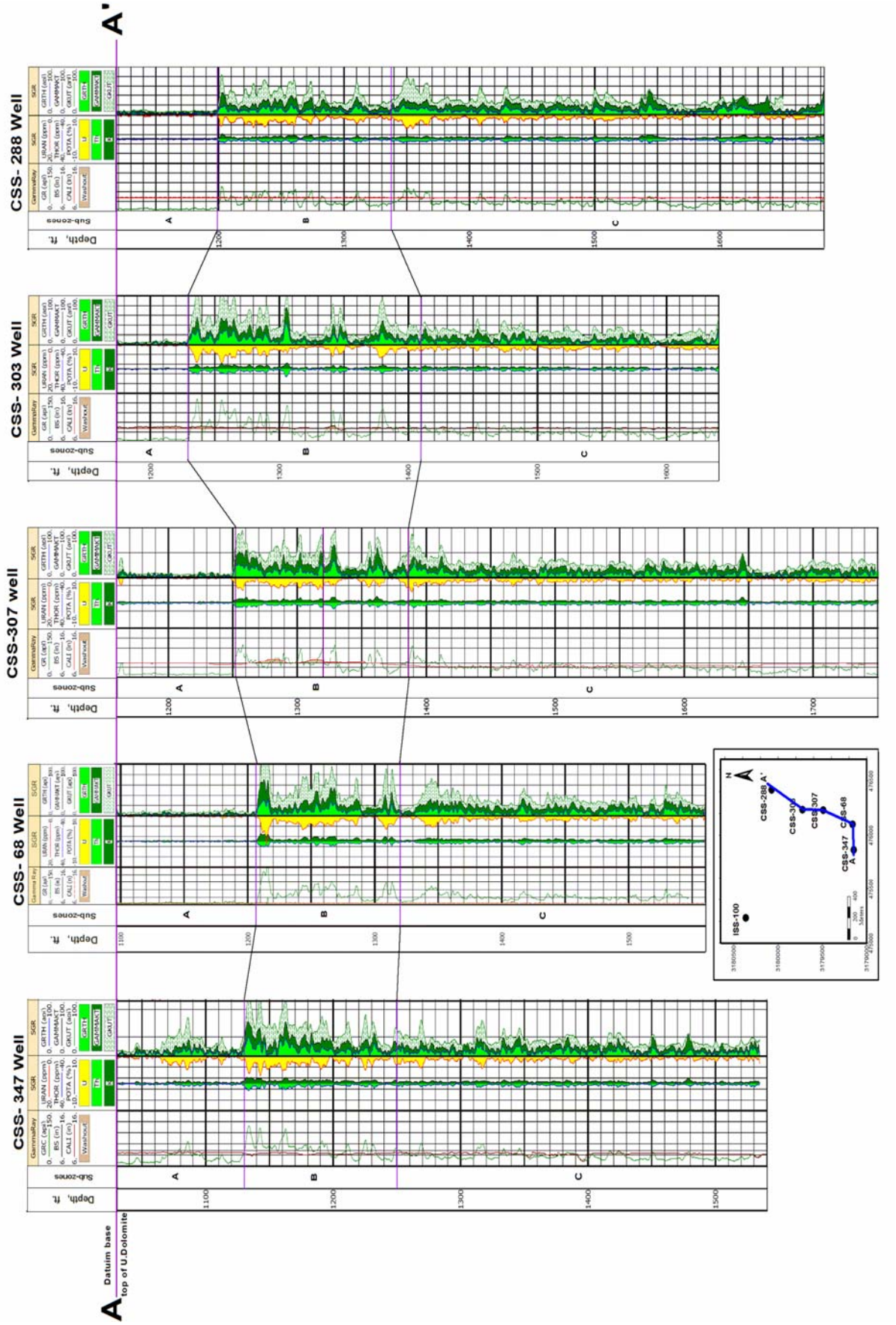

Fig. 15: Correlation of the study wells by using SGR signature of the upper dolomite rock unit, (Along A - A' Direction).

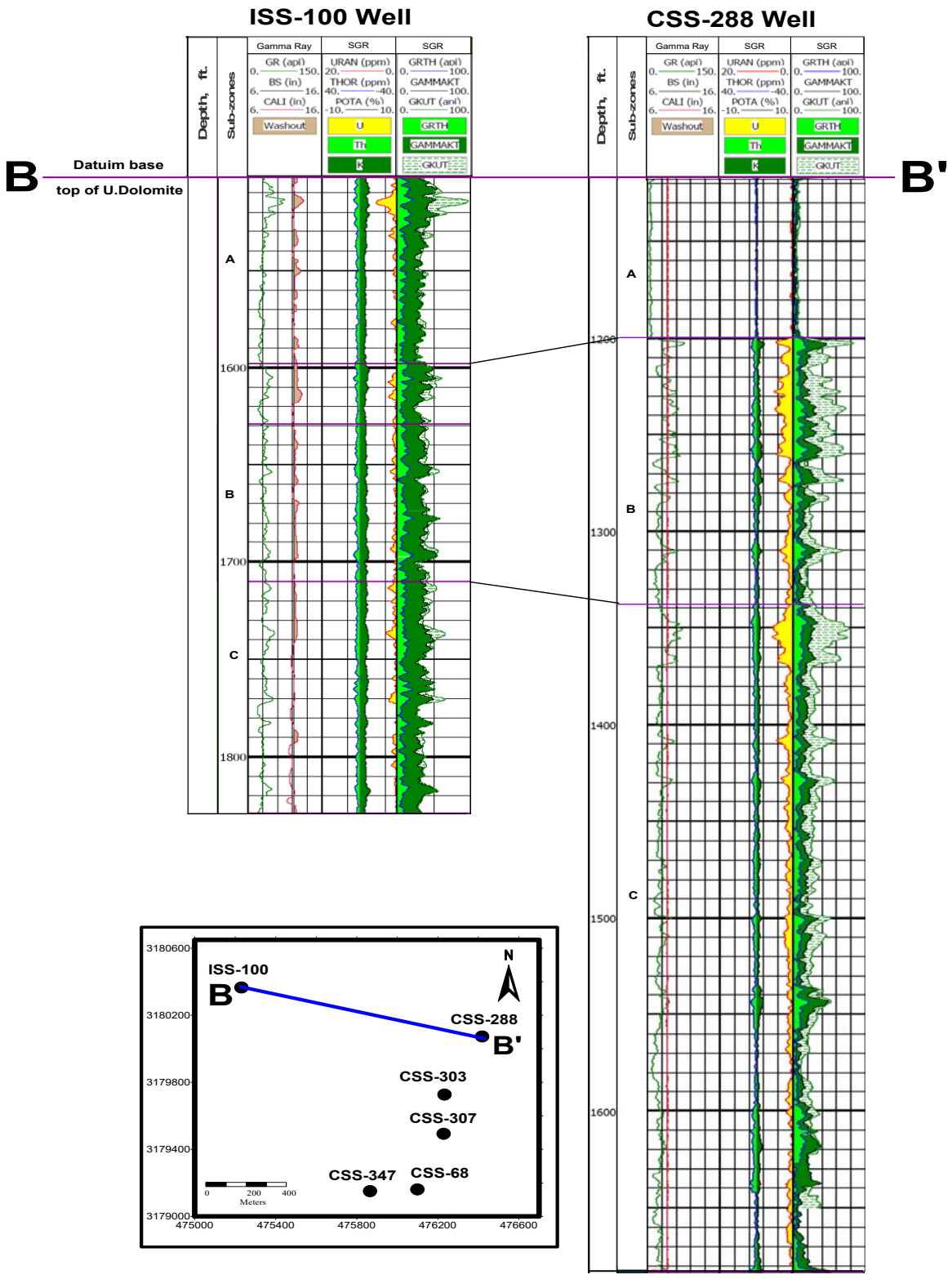

Fig. 16: Correlation of the study wells by using SGR signature of the upper dolomite rock unit, (Along B-B' Direction).

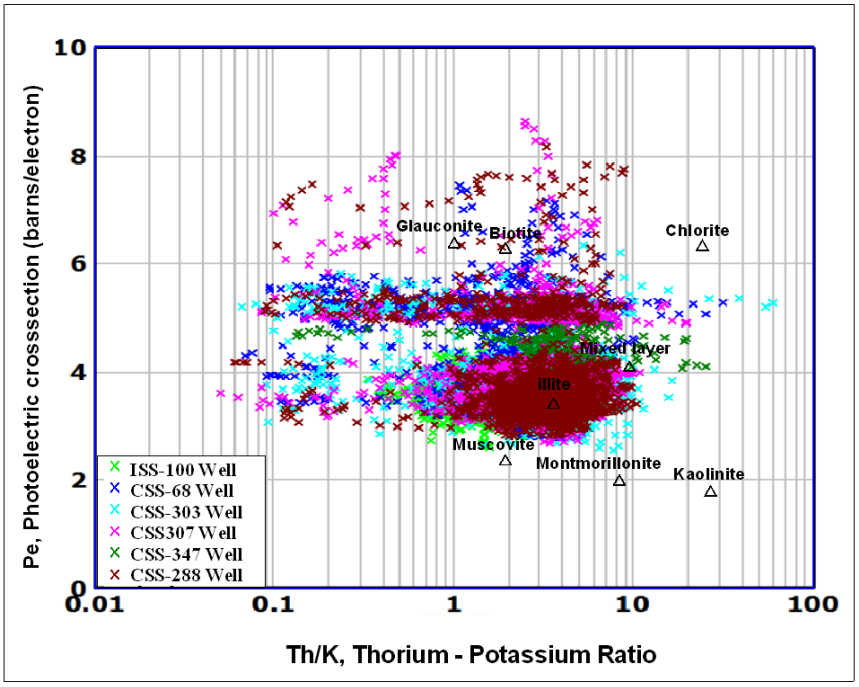

Fig. 17: Th/K ratio plotted against Pe for various clay types of the upper dolomite rock unit.

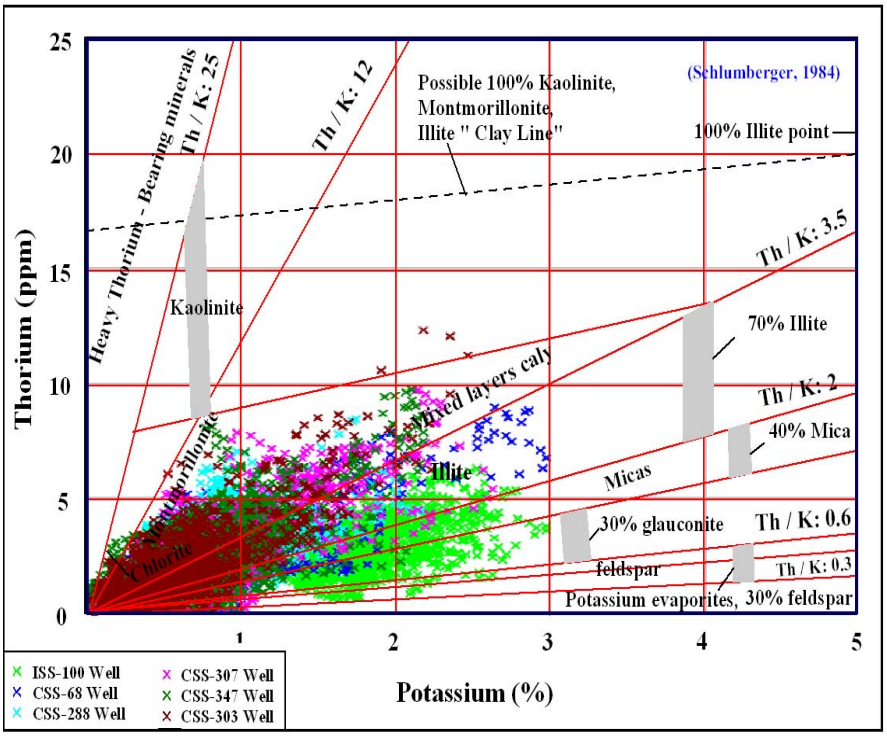

Fig. 18: Thorium-potassium cross-plot for mineral identification using spectral gamma ray data in the upper dolomite rock unit.

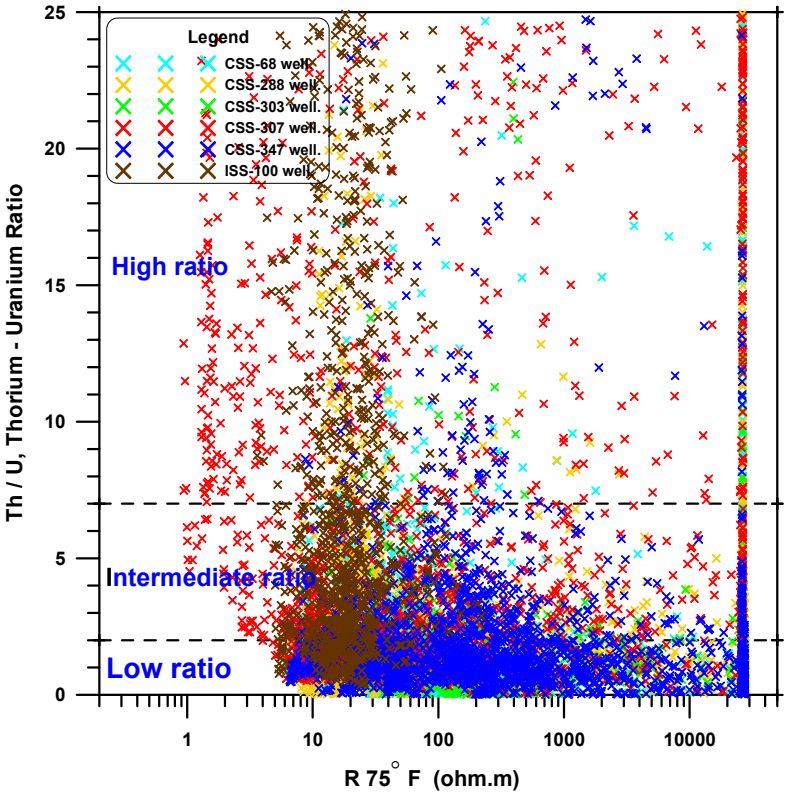

Fig. 19: Th/U ratio and resistivity crossplot of of the upper dolomite unit in the different wells of the studied area.

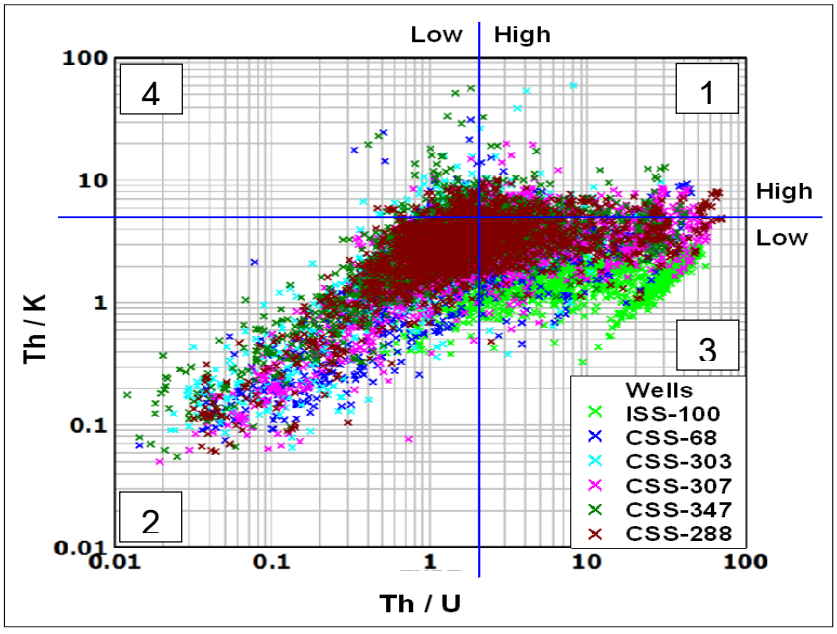

Fig. 20: Th/K ratio against Th/U ratio cross-plot for illustrating the depositional environments prevailing during the deposition of the upper dolomite rock unit.

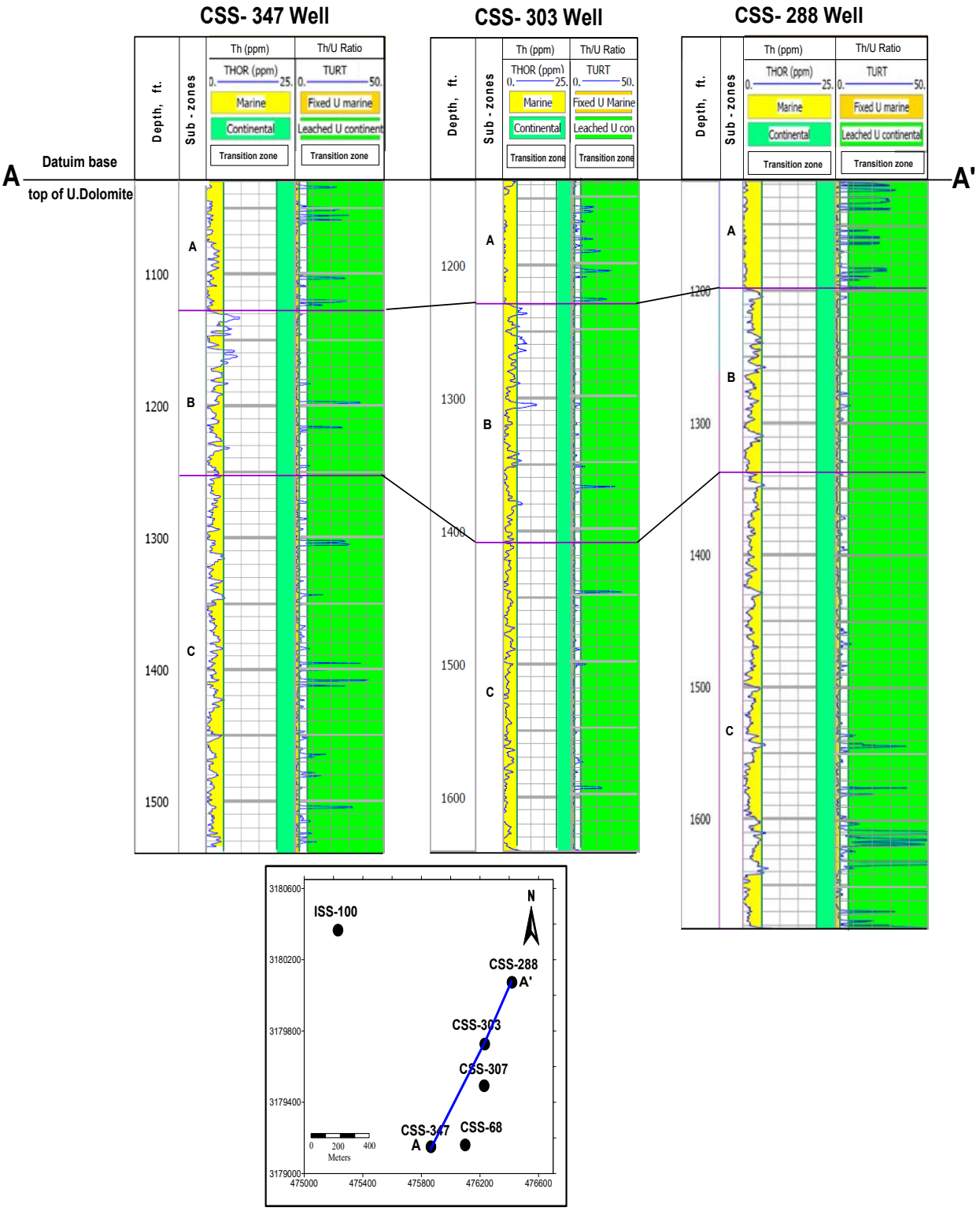

Fig. 21: Thorium and thorium-uranium ratio against depth, illustrating the depositional environments prevailing during the deposition of the upper dolomite rock unit.

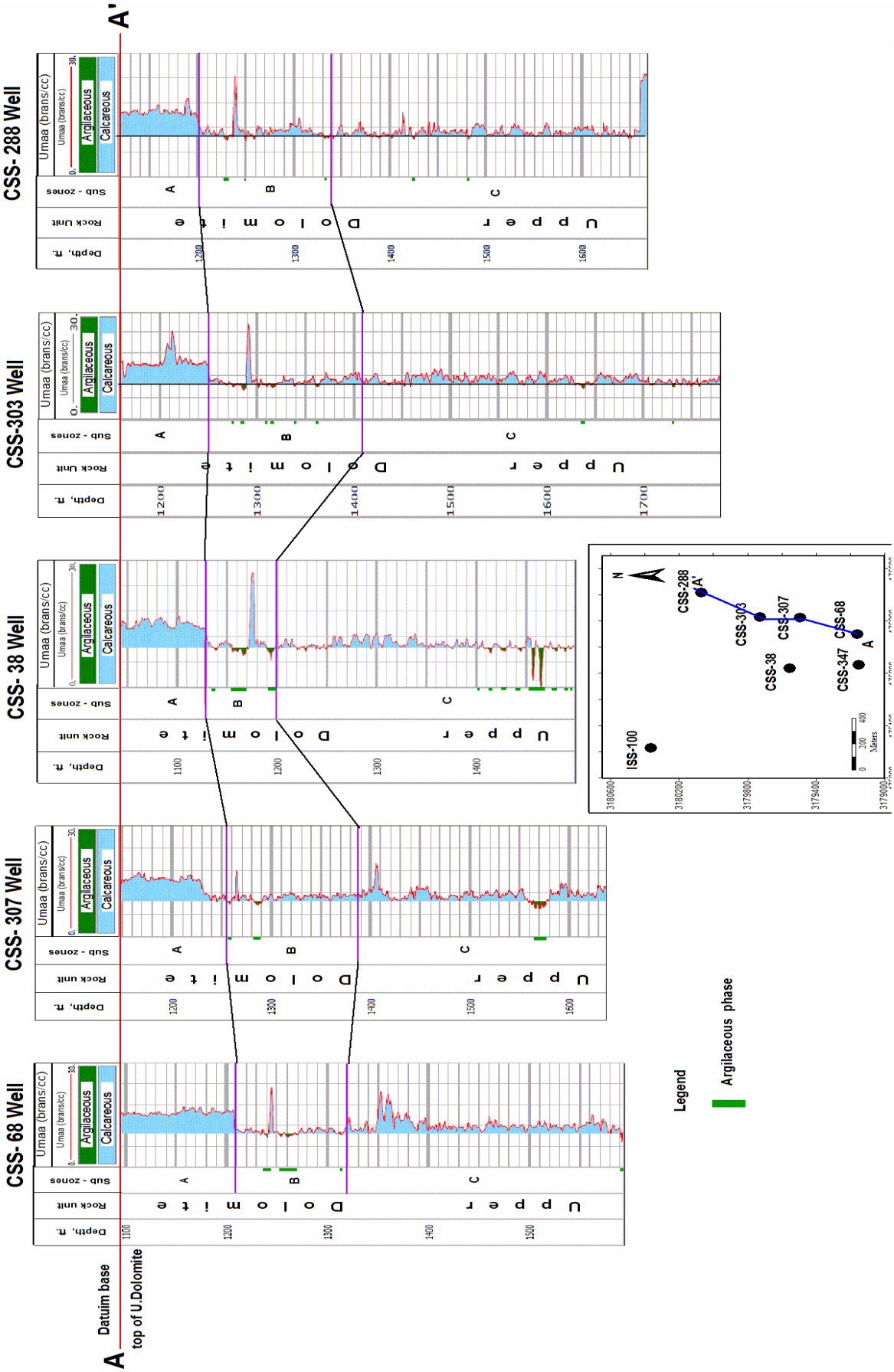

Fig. 22: A plot of Umaa versus depth indicating that, the upper dolomite rock unit sediments are mainly calcareous with minor argillaceous streaks.

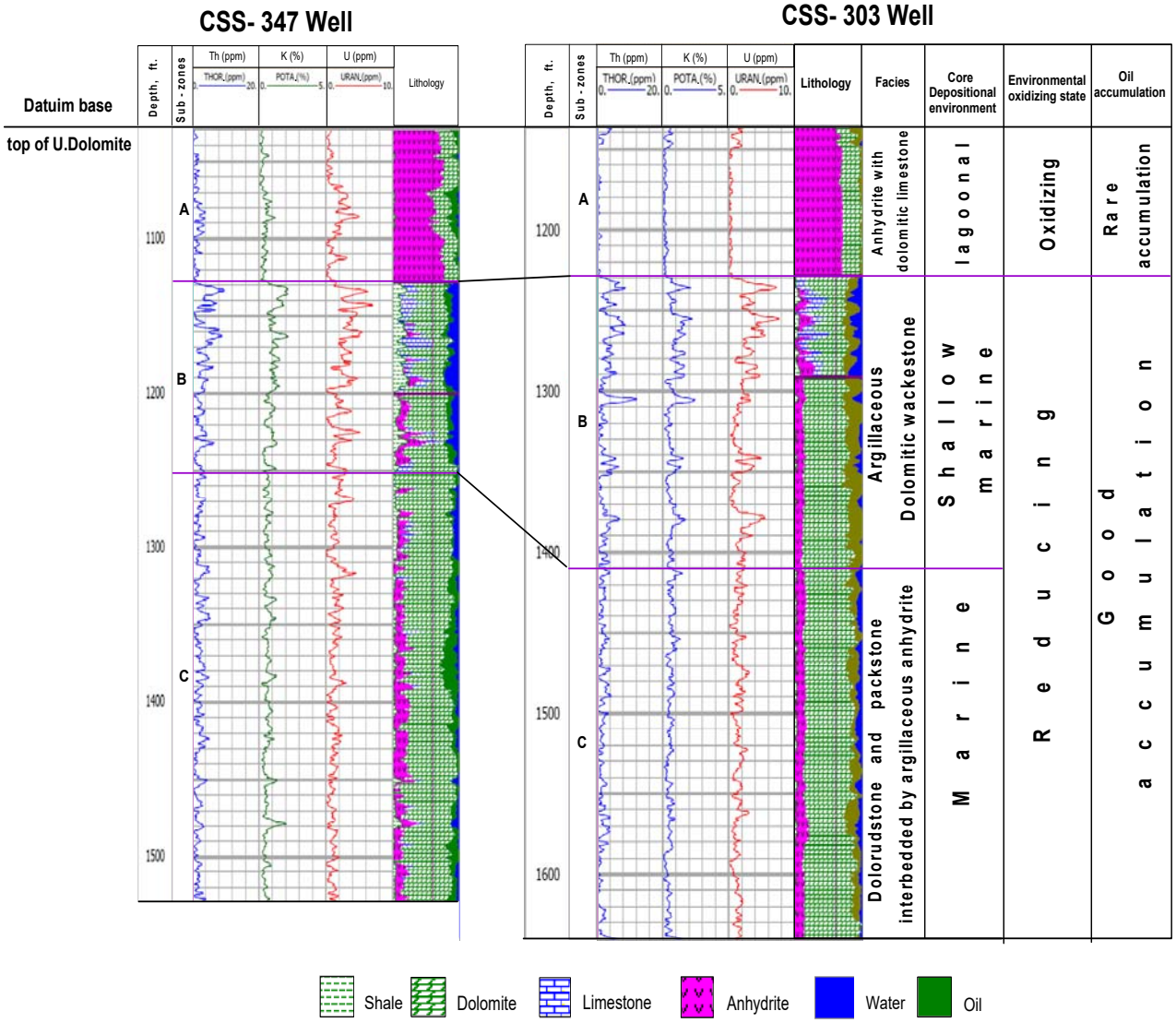

Fig. 23: Spectral gamma ray versus depth plot for the upper dolomite rock unit zones illustrating the facies variation and depositional condition.

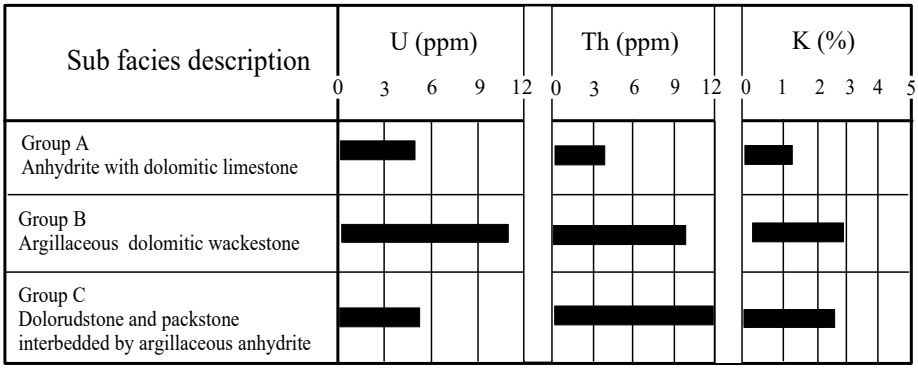

Fig. 24: A sketsh showing the SGR diagnostic values for the different facies in the upper dolomite rock unit.

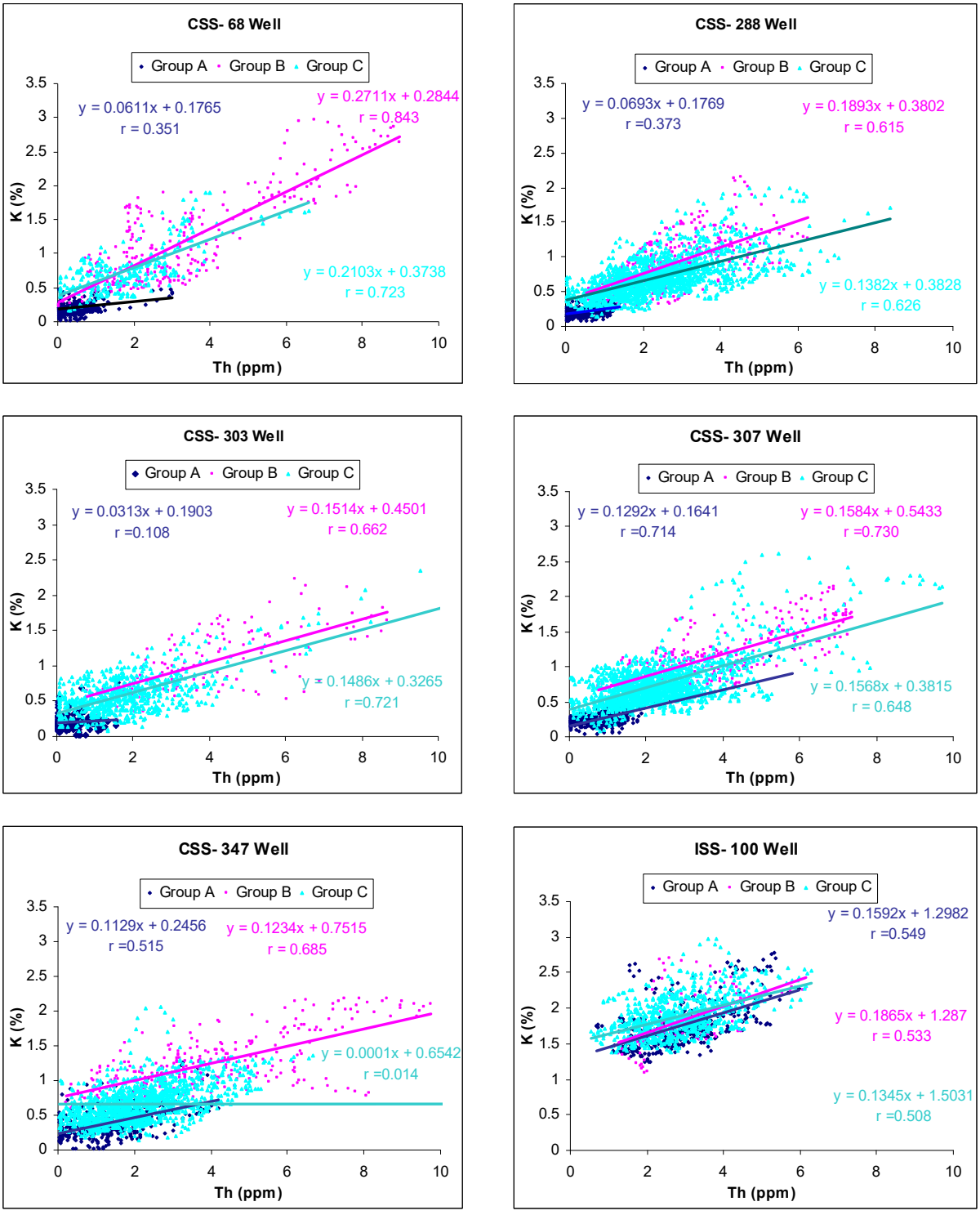

Fig. 25: X-Y Plots for Potassium (%) - Thorium (ppm) elements content of the upper dolomite rock unit in the different wells of the studied area.

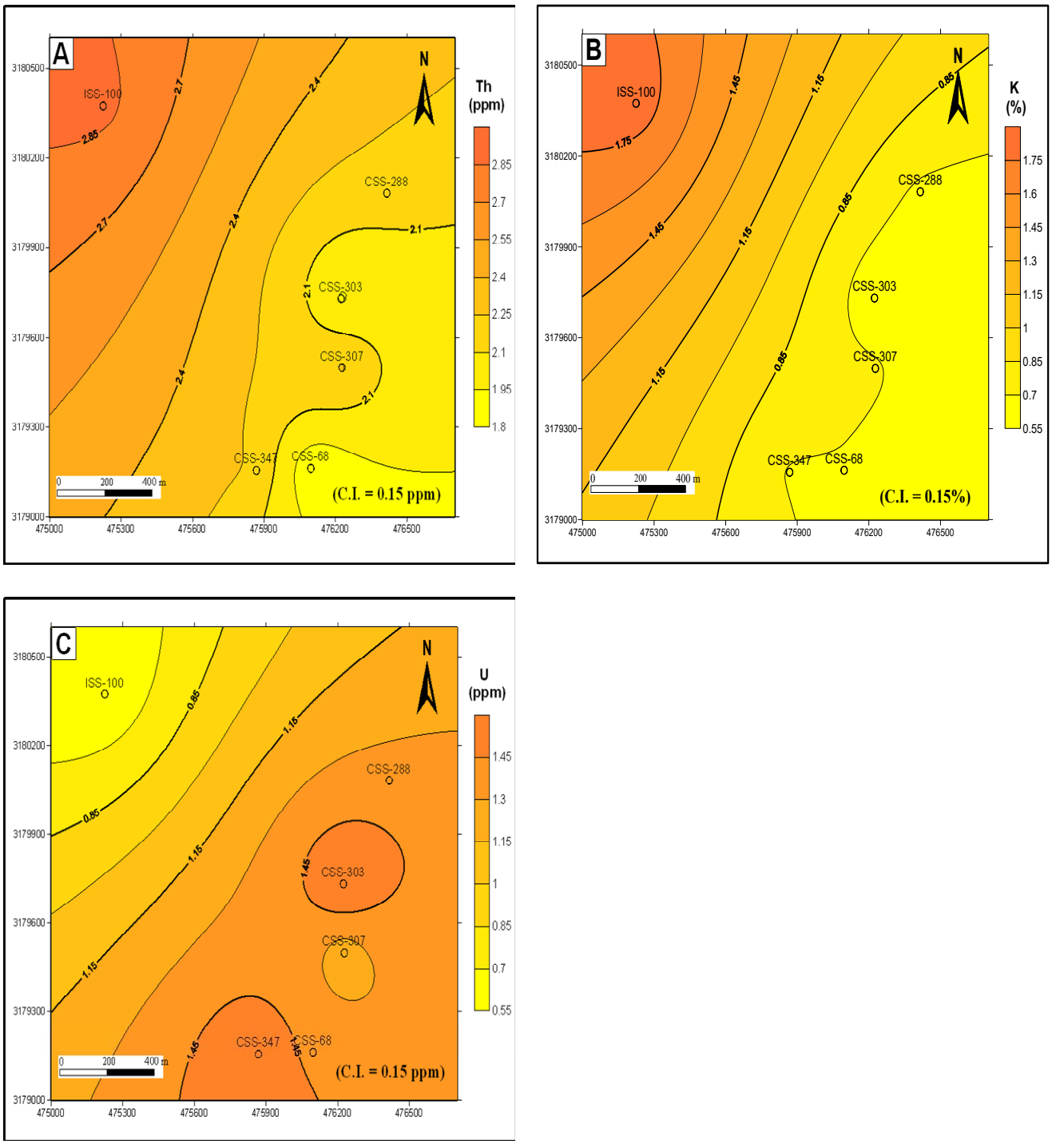

Fig. 26: Lateral distribution maps of SGR components in the study area, **A;** Thorium component map, **B;** Potassium component map and **C;** Uranium component map.

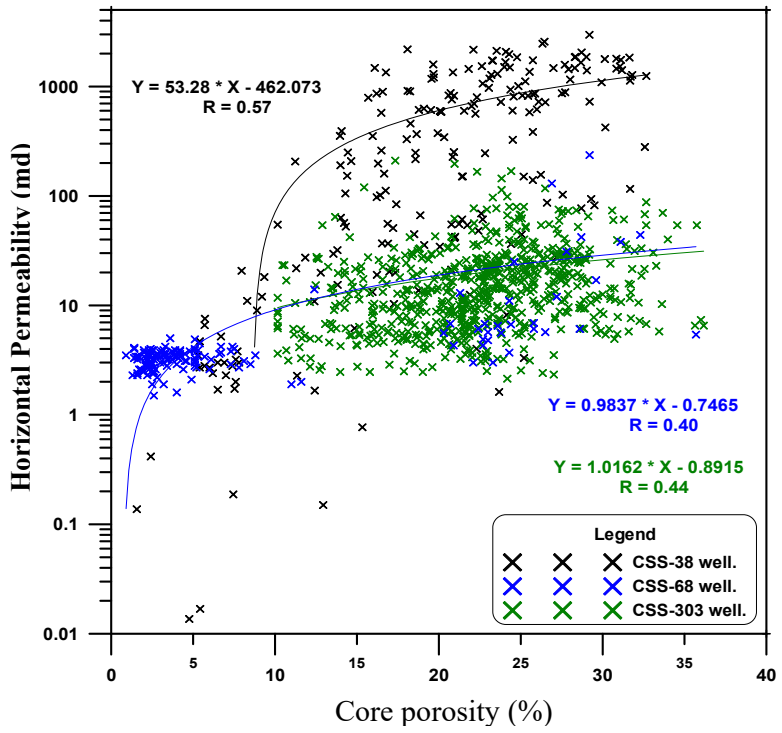

Fig. 27: Core-measured porosity versus core-measured horizontal permeability crossplot for the upper dolomite unit in CSS- 38, CSS-68 and CSS-303 wells.

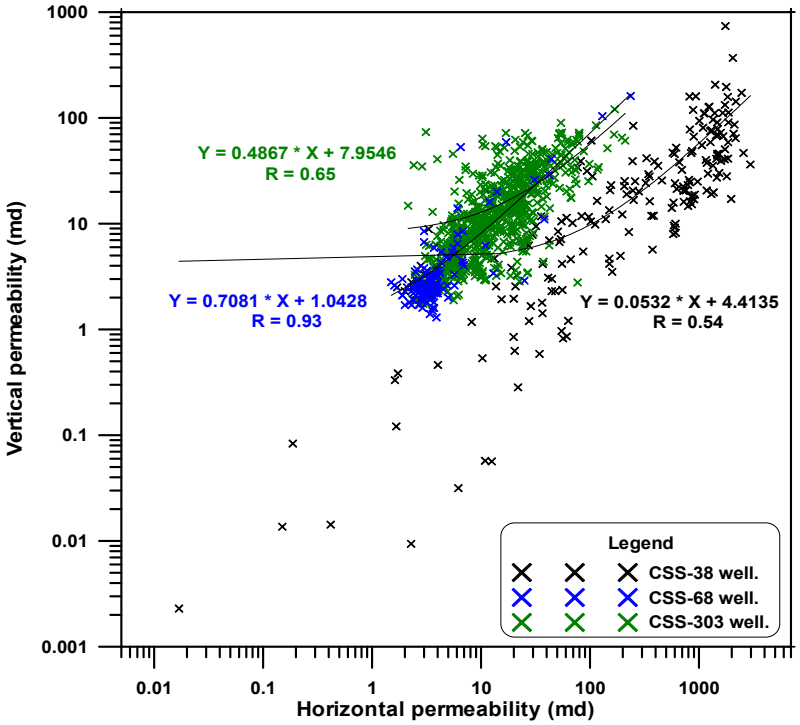

Fig. 28: The relation between vertical and horizontal permeability crossplot for the upper dolomite unit in CSS- 38, CSS-68 and CSS-303 wells.

International Journal of Scientific Engineering and Applied Science (IJSEAS) – Volume-5, Issue-3, March 2019
ISSN: 2395-3470
www.ijseas.com

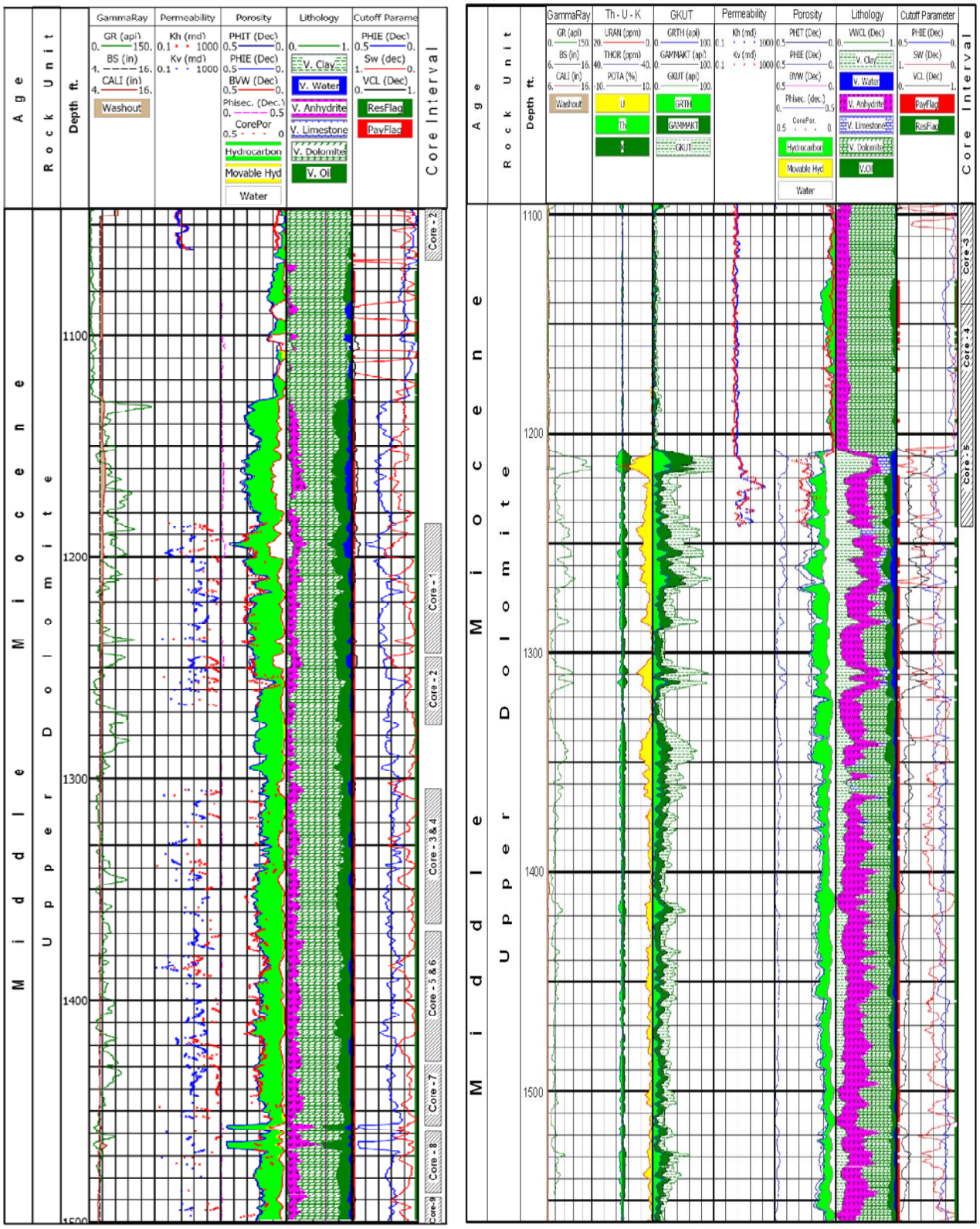

Fig. 29: Litho-saturation crossplot of upper dolomite rock unit, CSS-38 and CSS-68 wells.

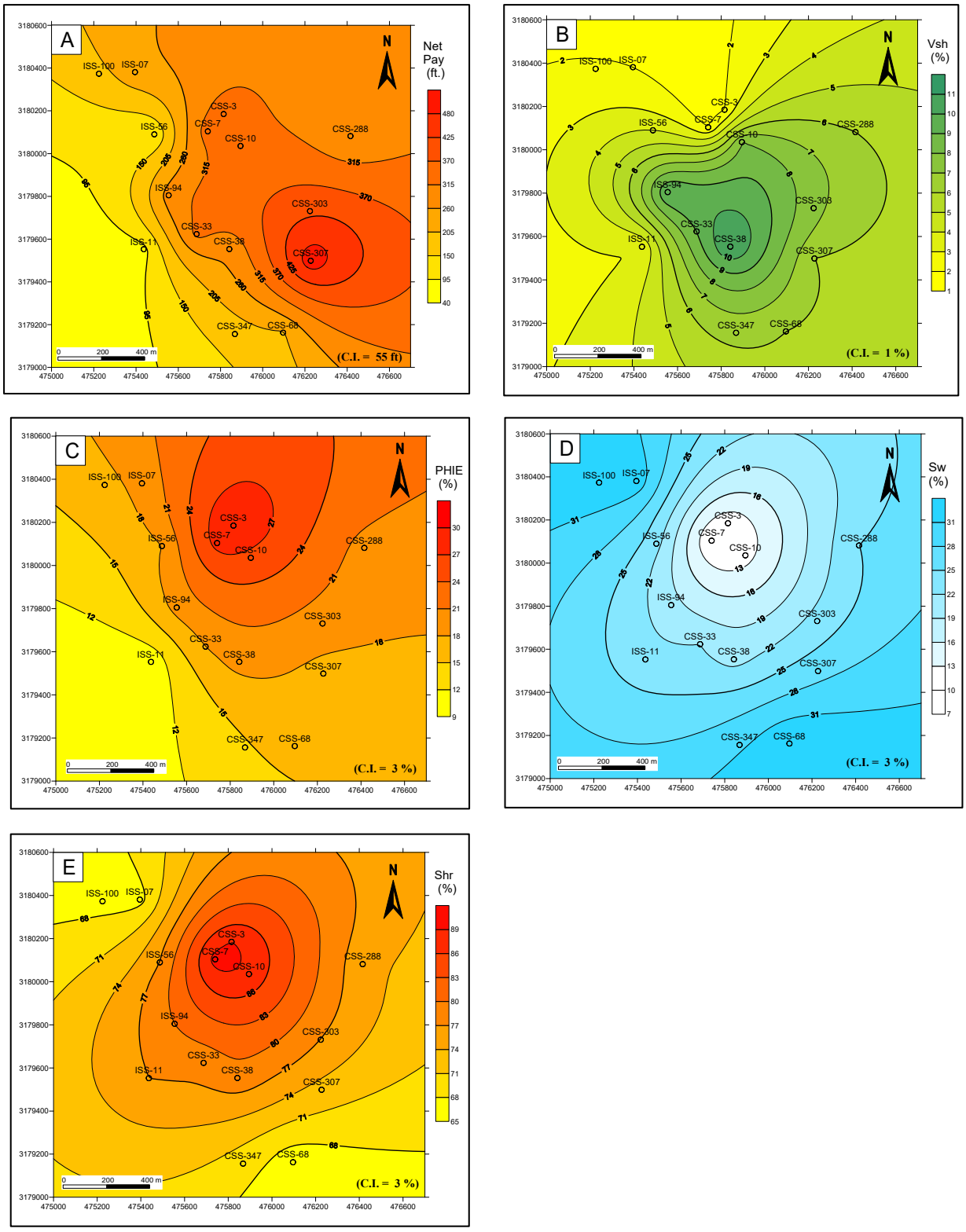

Fig. 30: Combined the petrophysical parameters of the upper dolomite rock unit in the study area, **A;** Net-pay thickness distribution map, **B;** Shale content distribution map, **C;** Effective porosity distribution map **D;** Water saturation distribution map and **E;** Hydrocarbon saturation distribution map.

References

Abd El-Rahman, A. Y. A. and Lashin, A., 2004. Evaluation of the Basement reservoir rocks in some selected wells in North Gulf of Suez and South Sinai, Egypt. Annals Geol. Surv. Egypt, V. XXVII, pp. 459-477.

Abu El Ela, M., Samir, M., Sayyouh, H. and ElTayeb, S., 2008. Thermal heavy-oil recovery projects succeed in Egypt, Syria. Oil & Gas journal, V. 106, Iss. 48.

Adams, J.A. and Weaver, C.E., 1958. Thorium-uranium ratios as indicators of sedimentary processes: example of concept of geochemical facies. AAPG Bull., V. 42(2), 43 P.

Ahr, W.M., 2005. Carbonate reservoir geology. Texas A&M Univ, College Station.

Alsharhan, A.S., 2003. Petroleum geology and potential hydrocarbon plays in the Gulf of Suez rift basin, Egypt. AAPG Bull. 87, pp.143-180.

Anders, M. H., Laubach, S. E., and Scholz, C. H., 2014. Microfractures: a review. Journal of Structural Geology 69, Part B, 377-394. doi: 10.1016/ j.jsg.2014.05.011.

Boyeldieu, C., and Winchester, A., 1982. Use of the Dual Laterolog for the evaluation of the fracture porosity in hard carbonate formations. In: Offshore South East Asia 1982 conference, 9–12 Feb.Singapore

Carr, I., Gawthorpe, R., Jackson, C., Sharp, I. and Sadek, A., 2003. Sedimentology and sequence stratigraphy of early syn-rift tidal sediments: the Nukhul Formation, Suez Rift, Egypt. Jour. Sed. Res., 75: pp. 407-420.

Davies, S.J. and Elliott, T., 1996. Spectral gamma-ray characterization of high resolution sequence stratigraphy: examples from Upper Carboniferous fluvio-deltaic systems, County Clare, Ireland. In: Howell, J.A., Aitken, J.F. (Eds.), High Resolution Sequence Stratigraphy: Innovations and Applications, Geological Society Special Publication, V. 104, pp. 25-35.

Dresser Atlas, 1982. Well Logging and Interpretation Techniques: The Course for home study. Dresser Atlas Division, Dresser Ind. Houston, TX, 350 pp.

Egyptian General Petroleum Corporation Stratigraphic Committee, 1964. Oligocene and Miocene rock stratigraphy of the Gulf of Suez Region. E.G.P.C., Cairo, 142 pp.

Egyptian General Petroleum Corporation Stratigraphic Committee, 1974. Miocene rock stratigraphy of Egypt, Journal of Egyptian Geological Society, 18, pp. 1-59.

Egyptian General Petroleum Corporation, 1996. Gulf of Suez oil and gas fields, Acomprehensive overview. Cairo, Egypt, pp. 520-528.

Ehrenberg, S.N., Svånå, T.A., 2001. Use of spectral gamma-ray signature to interpret stratigraphic surfaces in carbonate strata: an example from the Finnmark carbonate platform (Carboniferous-Permian), Barents Sea. AAPG Bull. 85 (2), pp. 295-308.

El Zarka, M. H. and Abdel Baki, M.A., 1989. Application of facies parameter to oil exploration or the subsurface Miocene Formation using a computer program. 1st Conf. Geochem. Fac. Sci., Alexandria Univ., Alexandria, Egypt, V. 3-4, pp. 537-566.

Essam, H., Ahmed, R., Heller, J., Kiefer, U. R., 2009. Issaran Field, Gulf of Suez, Egypt. Scimitar Production Egyptian LTD Internal report, 7 pp.

Evans, A. L., 1988. Neogene tectonic and stratigraphic events in the Gulf of Suez Rift area, Egypt. Tectanophysics, V.153, pp. 235-247.

Fertl, W. H., 1985. Gamma ray spectral data assists in complex formation evaluation, SPWLA 6th European Symp. Trans. Ldn, Paper Q, pp.1-32.

Fertl, W. H. and Rieke, H. H., 1985. Gamma ray spectral evaluation techniques identify fractured shale reservoirs and source rock characteristics, J. Pet. Tech., November, pp. 2053-2062.

Gamil, K., Ahmed, R., Saad, M. K., 2009. Petrographical report for CSS-38 well, Issaran Field, Gulf of Suez, Egypt. Scimitar Production Egyptian LTD Internal report.

Ghorab, M.A. and Marzouk, I.M., 1969. New Miocene rock stratigraphic units in Shukher - Rahmi area, Gulf of Suez (unpublished report, E.R.802).

Hassan, M., Hossi, A. and Combaz A., 1976. Fundamentals of the differential gamma ray log interpretation technique. SPWLA 17 th Ann. Symp. Trans., Paper H, 18 P.

Hassan, N. and Khalil, B. A., 1985. Petrophysical properties of Oligo – Miocene sediments in the october field, Abu Zenima, Gulf of Suez. 4th Annu. Meet, Egypt Geophys. Soc., Cairo, Egypt, pp. 259-279.

Kulke, H., 1982. A Miocene carbonate and anhydrite sequence in the Gulf of Suez as complex oil reservoir. 6th Pet. Expl. Seminar, E.G.P.C., Cairo, Egypt, V.1, pp. 269-275.

Khalil, B. and Mesheref, W.M., 1988. Hydrocarbon occurrences and structural style of the Southern Suez rift basin. Egypt. 9th Pet. Expl. and Prod. Conf., E.G.P.C., Cairo, Egypt, V. 1, pp. 86-109.

Khalil, S.M., McClay, K.R., 2001. Tectonic evolution of the NW red sea-Gulf of Suez rift system. In: Wilson, R.C.L., Whitmarsh, R.B., Taylor, B., Froitzheim, N. (Eds.), Non volcanic Rifting of Continental Margins: a Comparison of Evidence from Land and Sea. Geological Society, London, Special Publications, V. 187, pp. 453-473.

Khelifa, C., Zeddouri, A. and Djabes, F., 2014. Influence of natural fractures on oil production of unconventional reservoirs. Energy procedia, V. 50, pp. 360-367.

Koszy, F. F., 1956. Geochemistry of the radioactive elements in the ocean. Deep Sea Research, 3, 10 P.

Land, L.S., 1985. The origin of massive dolomite. J.geol. Edu., V.33, pp.112-125.

Laongsakul, P., Dürrast, H., 2011. Characterization of reservoir fractures using conventional geophysical logging. Songklanakarin, J. Sci. Techol., 33(2), pp.237-246.

Mackay, P. A., 2007. General Reef Corp., Calgary, AB, Canada. CSPG CSEG Convention.

Moustafa, A.R., 1997. Controls on the development and evolution of transfer zones: the influence of basement structure and sedimentary thickness in the Suez rift and Red Sea. Journal of Structural Geology V.19, pp. 755-768.

Moustafa A. A. E., 1976. Block Faulting in the Gulf of Suez. 5th Exploration Seminar, Cairo, Egypt, pp. 1-19.

Myers, K. J., and Wignall, P. B., 1987, Understanding Jurassic organic-rich mudrocks-new concepts using gamma-ray spectrometry and palaeoecology: examples from the Kimmeridge Clay of Dorset and the Jet Rock of Yorkshire, in J. K. Legget and G. G. Zuffa, eds., Marine clastic sedimentology: London, Graham and Trotman, pp. 172-189.

Patton, T. L., Moustafa, A. R., Nelson, R. A. and Abdine, A. S., 1994. Tectonic evolution and structural setting of the Gulf of Suez rift. In: Landon, S. M. (ed.) Interior Rift Basins. AAPG, Memoirs, 59, pp.9-55.

Poupon, A. and Gaymard, R., 1970. The evaluation of clay content from logs.Trans. SPWLA 11th Annual logging Symposium.

Rebson, D. A., 1971. The structural of the Gulf of Suez Clysmic rift with spcial reference to the Eastern side. Jouranl of Geological Society, V. 127, pp. 247 -276.

Richardson, M. and Arthur, M. A., 1988. The Gulf of Suez-northern Red Sea Neogene rift: A quantative basin analysis. Marine and Petroleum Geology, V. 5, pp. 247-270.

Said, R., 1962. The Geology of Egypt; Elsevier, Amsterdam – New York, 337pp.

Said, R., 1990. The Geology of Egypt. E.G.P.C., CONOCO, Hurghada Inc. and Repsol Expl. S. A., 734 pp.

Saller, A. H., Dickson, J. A. D. and Boyd, S. A., 1994. Cycle stratigraphy and porosity in Pennsylvanian and Lower Permian shelf limestones, eastern Central Basin platform, Texas: AAPG Bulletin, v. 78, pp. 1820-1842.

Samir, M., 2010. Rejuvenation Issaran Field - Case study.SPE 127847, 14 pp.

Saoudi, A., Moustafa, A. R., Farag, R. I., Omara, M. M., Wally, H., Fouad, A., Tag, A., and Ragab, R. Z., 2012. Dual-porosity fractured Miocene syn-rift dolomite reservoir in the Issaran Field (Gulf of Suez, Egypt): a case history of the zonal isolation of highly fractured water carrier bed Geological Society, London, Special Publications, 374, first published on September 5, 2012, doi:10.1144/SP374.7

Schlumberger, 1974. Log Interpretation, V.II - Applications. Schlumberger Limited, New York, N.Y. 10017, U.S.A., 116 p.

Schlumberger, 1989. Log Interpretation Principles / Applications. Schlumberger Educational Services, Houston, Texas, U.S.A., 236 p.

Sellwood, B. W. and Netherwood, R. E., 1984. Facies Evaluation of the Gulf of Suez area Sedimentary History as indicator of rift Initiation and development. Modern Geology, V.9, pp. 43 - 69.

Serra, O. and Serra, L., 2004. Well Logging: Data Acquisition and Applications. Editions Technip, pp. 674.

Sibbit, A. M. and Faivre, O., 1985. The Dual Laterolog response in fractured rocks, SPWLA. In: 26th Ann Log Symp. Trans Paper T

Swanson, V. E., 1961. Geology and geochemistry of uranium in marine black shales, a review: U.S. Geological Survey Professional Paper 356-C, pp. 67-112.

Tawfik, N.M., 1988. Exploration outlook on the northern Gulf of Suez, Egypt. 9th Petrol. Expl. and Prod. Conf., E.G.P.C., Cairo, Egypt, 26 pp.

Tucker, M.E. and Wright, V.P., 1990. Carbonate sedimentology" Black well Sc., Publ., 482 pp.

Tucker, M.E., 2001. Sedimentary Petrology. 3rd Black well Science Ltd., Osney Nead, Oxford OX2 0EL, UK; 262 pp.

Zuhair, A., Hussain, A. and Mohammed, A., 2014. An overview of steam injection projects in fractured carbonate reservoirs in the Middle East. Journal of Petroleum Science Research (JPSR) V. 3, Issue 3, 58 pp.

Youssef, A., 1986. Coastal to shallow marine Miocenc facies in Zeit Bay area, Gulf of Suez. 8th E.G.P.C. Exploration Seminar. Egypt, v. 1, p.344-359.